COMPARISON AND CORRECTION OF MULTISTAGE TRIAXIAL TESTS TO SINGLE STAGE TRIAXIAL TEST FOR THE ROCK MECHANICAL TESTING

A Thesis

Presented to

the Department of Petroleum Engineering

University of Houston

In Partial Fulfillment

of the Requirements for the Degree

Master of Science

By

Malik Alsalman

May 2015

COMPARISON AND CORRECTION OF MULTISTAGE TRIAXIAL TESTS TO SINGLE STAGE TRIAXIAL TEST FOR THE ROCK MECHANICAL TESTING

Malik Alsalman

Approved:

Dr. Michael Myers, Associate Professor,
Chair of the Committee, Cullen College
of Engineering

Committee Members:

Dr. Lori Hathon, Associate Professor,
Petroleum Engineering Department

Dr. Kaspar Willam, Associate Professor,
Civil Engineering Department

Dr. Suresh K. Khator, Associate Dean,
Cullen College of Engineering

Dr. Tom Holley, Professor and Director,
Petroleum Engineering Department

Acknowledgements

I would like thank my committee chair, Dr. Michael Myers, for assisting me with writing and evaluating my thesis. Dr. Myers was very supportive by allowing me to use his equipment for my work.

I would like to thank Metarock Laboratories and their staff especially the owner, Munir Aldin, who allowed me to use his laboratory equipment to perform part of my tests. In addition, I would like to thank the lab CEO, Samir Aldin, for his allowence to use the lab facility and Omer Abdulbaki for his technical support.

COMPARISON AND CORRECTION OF MULTISTAGE TRIAXIAL TESTS TO SINGLE STAGE TRIAXIAL TEST FOR THE ROCK MECHANICAL TESTING

An Abstract of a Thesis

Presented to

the Department of Petroleum Engineering

University of Houston

In Partial Fulfillment

of the Requirements for the Degree

Master of Science

By

Malik Alsalman

May 2015

Abstract

In this work, we investigate the relationship between two test protocols; the Single Stage Triaxial (SST) is where a constant confining stress is applied and the axial stress is raised until the sample fails. This is compared to the Multistage Triaxial (MST) test, where the sample is loaded to the point of positive dilatency (PPD) then unloaded to low deviatoric stress, the confining stress raised and the procedure repeated. We have performed these measurements for several different types of rocks (Shale, Sandstone, and Chalk) and compared the results in terms of Young's modulus, Poisson's ratio, stiffness, friction angle, and cohesion. We provide a detailed discussion of the techniques and measurements required to correct the MST results to those obtained from SST protocol. A single correction factor is found to relate the MST results to the SST. Future work is proposed to further develop the measured parameters from these two test protocols.

Table of Contents

List of Figures

List of Tables

Chapter 1 : Introduction

1.1 The Stress-Strain Curve

When a loading force is applied to a rock, it typically exhibits a linear stress /strain response dominated by recoverable strains i.e., the elastic region. As the force is increased, more ductile behavior (larger irrecoverable strains) is observed until the rock “fails”. As typically, the stress/strain response is dived into three regions. **Figure 1.1** shows the typical behavior of the rock when applying an axial load on it. In this case a brittle failure where the sample can no longer support any deviatoric stress.

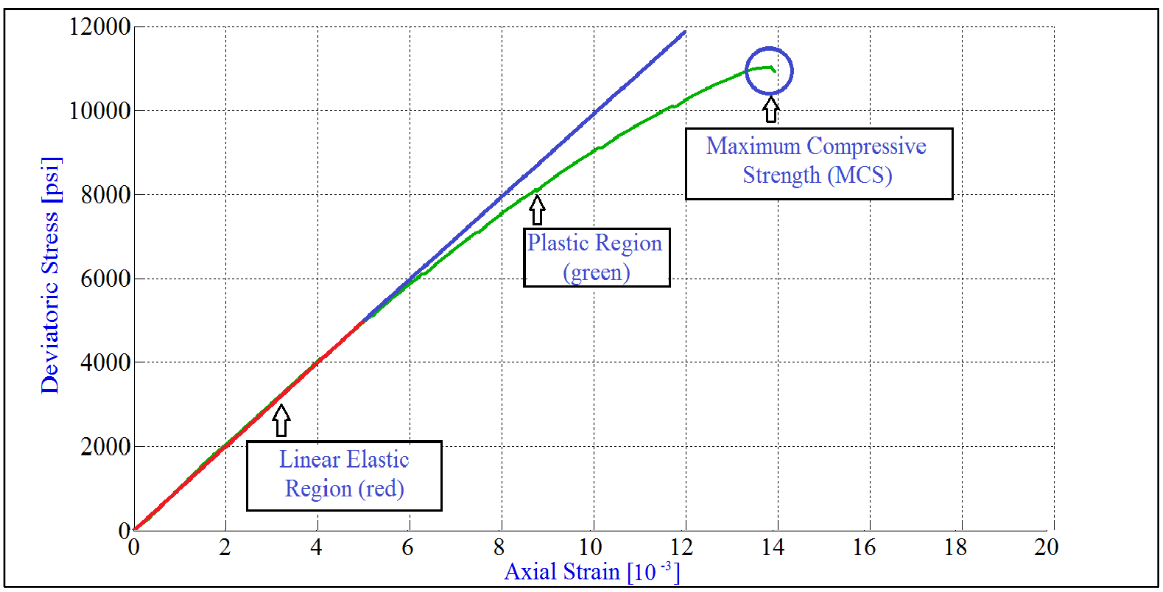

Figure 1.1: Typical behavior of rock under axial stress where it has three modes; linear elastic, plastic (deviates from a linear response), and failure.

1.1.1 Stress Tensor in Two Dimensions and Determination of the Principal Stresses

In this section we define the stresses that are relevant to the axisymmetric rock mechanics tests we performed. We used cylindrical plug and equipment that allow differing axial and the confining (radial stress) stresses to be applied. Because of the radial symmetry we need only be concerned with two stresses, which we will resolve into the normal and shear stress relative to any defined plane in the sample. To do this we will be using the concept of Mohr's stress circle.

To derive the relevant equations, let us start with the cross section in x-y plane as shown in **Figure 1.2**, by assuming a plane oriented to x direction with angle (θ) and has a normal stress (σ_n) and component along the plane, the shear stress (τ) . Let us start by taking the upper triangle as shown in **Figure 1.3** and applying force analysis to find the components that are parallel to normal stress and the shear stress, at the force equilibrium, the equations become as follows.

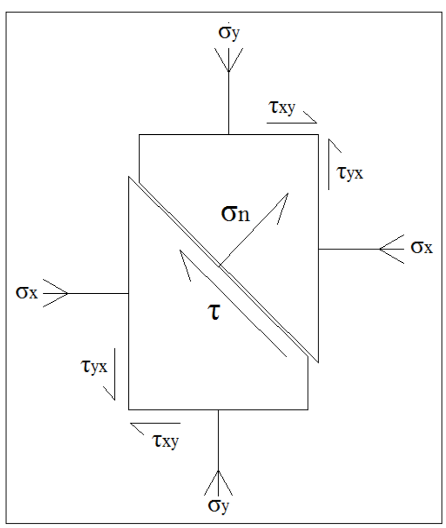

Figure 1.2: A rock sample induced to axial and radial stress.

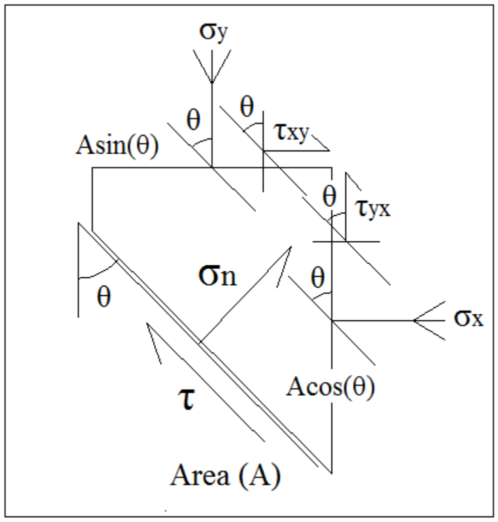

Figure 1.3: Stress analysis on a rock sample for applied axial (σ_y) and radial (σ_x) stresses.

For the normal stress,

$$\sigma_n * A = \sigma_x sin(90-\theta) * A * cos\theta + \sigma_y * sin\theta * A * sin\theta + \tau_{xy} * sin(90-\theta) * A * sin\theta + \tau_{yx} * sin\theta * A * cos\theta. \qquad 1.1$$

We assume that $\tau_{xy} = \tau_{yx}$ (the object is in equilibrium). With some simple trigonometry Eqn. (1.1) becomes:

$$\sigma_n = \sigma_x \cos^2\theta + \sigma_y \sin^2\theta + 2\tau_{xy} cos\theta sin\theta, \qquad 1.2$$

and applying the half angle theorem,

$$\sigma_n = \sigma_x \cos^2\theta + \sigma_y \sin^2\theta + \tau_{xy} sin2\theta. \qquad 1.3$$

For the shear stress

$$\tau * A = -\sigma_x sin\theta * A * cos\theta + \sigma_y \cos\theta * A * sin\theta + \tau_{xy} * \cos(90-\theta) * A * sin\theta - \tau_{yx} * cos\theta * Acos\theta \quad and \qquad 1.4$$

$$\tau = -\sigma_x sin\theta cos\theta + \sigma_y sin\theta cos\theta + \tau_{xy}(\cos^2\theta - \sin^2\theta). \qquad 1.5$$

Recalling that,

$$\cos^2\theta = 0.5(cos2\theta + 1), \qquad 1.6$$

$$\sin^2\theta = 0.5(1 - cos2\theta)\,, and \qquad 1.7$$

$$sin2\theta = 2sin\theta cos\theta. \qquad 1.8$$

Then the normal and shear stresses resolved into a plane at angle *(θ)* from the vertical,

$$\sigma_n = \frac{1}{2}(\sigma_x + \sigma_y) + \frac{1}{2}(\sigma_x - \sigma_y)cos2\theta + \tau_{xy}sin2\theta \; and \qquad 1.9$$

$$\tau = -\frac{1}{2}(\sigma_x - \sigma_y)sin2\theta + \tau_{xy}cos2\theta. \qquad 1.10$$

The principal stress directions are defined as the angle of the plane where the shear stress is zero, i.e.,

$$0 = -\frac{1}{2}(\sigma_x - \sigma_y)sin2\theta + \tau_{xy}cos2\theta. \qquad 1.11$$

Solving for the angle:

$$\theta = \frac{1}{2}\tan^{-1}\left(\frac{\tau_{xy}}{0.5(\sigma_x - \sigma_y)}\right). \qquad 1.12$$

Substituting (1.12) into (**1.11** and **1.17**), and solving for the stresses gives the magnitudes of the principal stresses which are:

$$\sigma_1 = \frac{1}{2}(\sigma_x + \sigma_y) + \sqrt{\tau_{xy}^2 + \frac{1}{4}(\sigma_x - \sigma_y)^2} \ and \qquad 1.13$$

$$\sigma_2 = \frac{1}{2}(\sigma_x + \sigma_y) - \sqrt{\tau_{xy}^2 + \frac{1}{4}(\sigma_x - \sigma_y)^2}. \qquad 1.14$$

1.1.2 Mohr's Stress Circle

For axisymmetric test performed in this study the confining stress and the axial stress are orthogonal to each other and Therefore, ($\tau_{xy} = \tau_{yx} = 0$), equations (1.9) and (**1.10**) can be simplified to :

$$\sigma_n = \frac{1}{2}(\sigma_x + \sigma_y) + \frac{1}{2}(\sigma_x - \sigma_y)cos2\theta, \qquad 1.15$$

$$\left(\sigma_n - \frac{1}{2}(\sigma_x + \sigma_y)\right) = \frac{1}{2}(\sigma_x - \sigma_y)cos2\theta, and \qquad 1.16$$

$$\tau = -\frac{1}{2}(\sigma_x - \sigma_y)sin2\theta. \qquad 1.17$$

Squaring (**1.16**), (1.17) and add them together, we get the equation of circle:

$$\left(\sigma_n - \frac{1}{2}(\sigma_x + \sigma_y)\right)^2 + \tau^2 = \left(\frac{\sigma_y - \sigma_x}{2}\right)^2. \qquad 1.18$$

Equation (1.18) shows that the normal stress is related to the shear stress by a circle which is called the Mohr's circle as shown in **Figure 1.4**. It has a center point of $(\sigma_x + \sigma_y)/2$ and a radius of $(\sigma_x - \sigma_y)/2$.

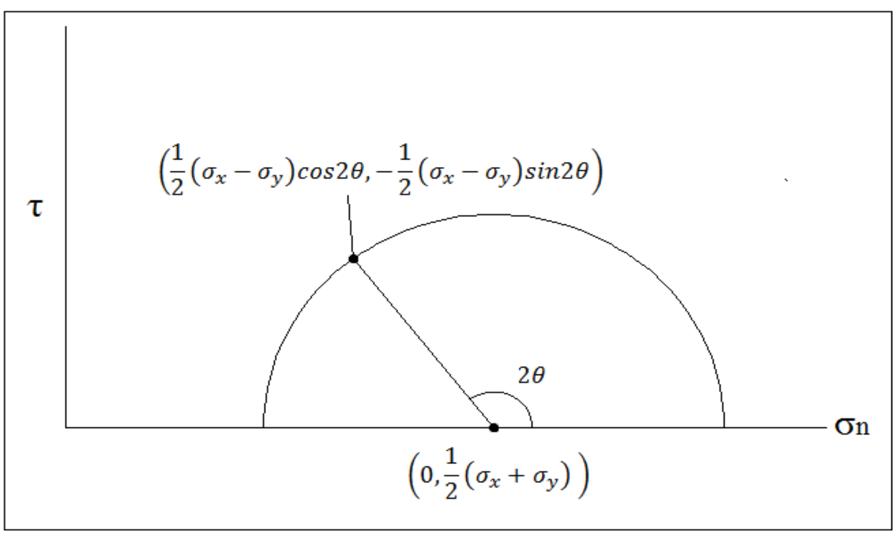

Figure 1.4: Mohr circle that shows the stresses applied to the rock sample.

For a plane angle (θ) the, shear stress and normal stress correspond to a point on Mohr's circle. The maximum shear stress occurs when either (θ) equals to 45° or 135°. Also, the maximum normal stress occurs when (θ) equals to 0° or 90°. This happens when the plane is orthogonal either to (σ_x) or (σ_y).

1.1.3 Rock Failure and Mohr-Coulomb Criteria

Let us assume the sample is subjected to an axial load as shown in Figure **1**.**2**, as the stress increases until it cannot support further loading. This point is called a maximum compressive strength (MCS). Three types of failure are experienced by the rock sample when a stress is applied on it, these types are as follows:

Tensile failure: this type of failure occurs when tensile stresses are applied to the sample. The sample then reach a critical limit called the maximum tensile stress. **Figure 1.5** show the tensile failure of the rock sample where it is separated apart as reaching the tensile failure.

Shear failure: this type occurs when compressive stresses are applied to the sample. The sample reaches a critical limited called the maximum compressive strength, it fails and the results is two parts sliding on an plan (fault zone) with a specific angle as shown in Figure **1**.**3**. The shear failure is presented **Figure 1.6** where the broken parts of the rock slide on an oriented plan.

Compaction failure: this happens in very porous media where the pore space collapses due to the increase of isostatic effective stress applied to the sample. When the compaction occurs, the grains break and reoriented to fill the pore space. The result is a new compacted sample that has smaller dimensions.

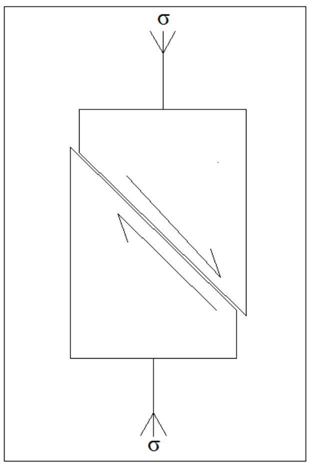

Figure 1.6: Shear failure as the rock has two parts slides on an oriented plan.

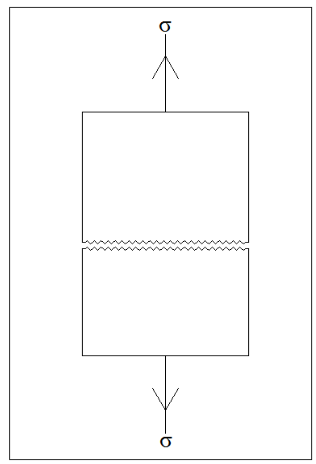

Figure 1.5: Tensile stress where the rock fails into two pieces.

Mohr-Coulomb Criterion

In shear failure, which this thesis deals with, as the failure zone occurs and the two parts move along this zone. The simplest assumption for the relation between the applied stresses at failure is the Mohr-Coulomb criterion which states that there is a linear relation between the normal stress (σ_n) and the shear stress (τ) (**Figure 1.2**) as follows:

$$\tau = \mu\, \sigma_n + C_o\,. \qquad 1.19$$

Recalling from the basic physics related to friction force, the factor (μ) is the friction coefficient related to the applied normal stress, and (C_o) is called the inherent shear stress that represents the cohesion of the sample along the sliding plan. **Figure 1.7** shows the graphical representation of the criterion using Mohr circle where the assumption is made that the friction angle related to the friction coefficient (μ) is constant.

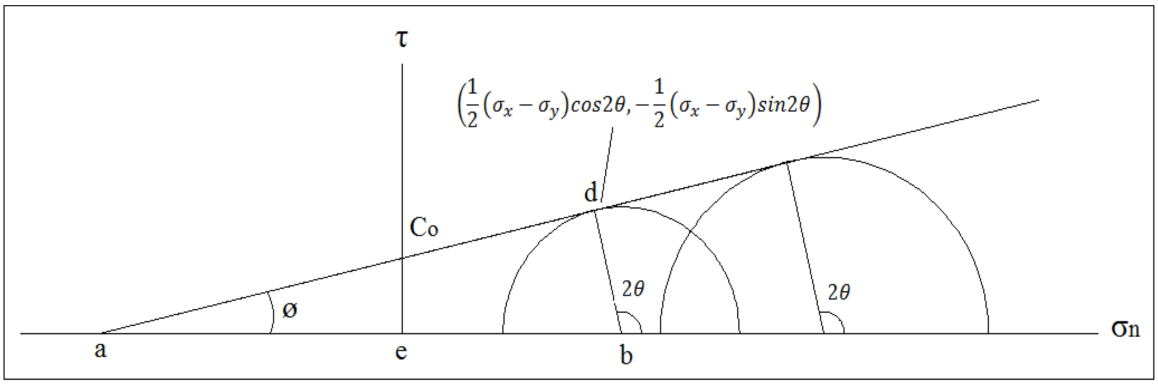

Figure 1.7: Graphical representation of Mohr-Coulomb criterion using Mohr circle.

One problem related to this graph, is that both (σ_n) and (τ) can't be measured directly in the laboratory. In contrast, (σ_x) and (σ_y) can be measured directly from the test. Therefore, a conversion should be made to (**1.19**) to be in terms of (σ_x) and (σ_y) in order to calculate the friction angle and cohesion of the sample which is the main aim of performing the rock mechanic tests in the laboratory. Referring to the right triangle (adb) in **Figure 1.7**, the model (1.19) can be converted as

$$ab = ae + eb, \qquad 1.20$$

$$\theta = 45 - \phi/2, \quad 1.21$$

$$sin\phi = \frac{db}{ab}, \quad 1.22$$

$$tan\phi = \frac{C_o}{ae}, and \quad 1.23$$

$$eb = \left(\frac{\sigma_x + \sigma_y}{2}\right). \quad 1.24$$

Therefore,

$$ab = \frac{db}{\sin\phi} = \left(\frac{\sigma_x + \sigma_y}{2}\right) + C_o cot\phi, \quad 1.25$$

$$db = \left(\frac{\sigma_x + \sigma_y}{2}\right) sin\phi + C_o cos\phi, \quad 1.26$$

db =

$$\sqrt{\left(\frac{1}{2}(\sigma_x - \sigma_y)cos2\theta + \left(\frac{\sigma_x + \sigma_y}{2}\right) - \left(\frac{\sigma_x + \sigma_y}{2}\right)\right)^2 + \left(\frac{1}{2}(\sigma_x - \sigma_y)sin2\theta\right)^2}. \quad 1.27$$

Simplifying (**1**.**27**), then db becomes:

$$db = \left(\frac{\sigma_y - \sigma_x}{2}\right) = \left(\frac{\sigma_x + \sigma_y}{2}\right) sin\phi + C_o cos\phi, \quad 1.28$$

which has the following general from

$$\left(\frac{\sigma_y - \sigma_x}{2}\right) = m\left(\frac{\sigma_x + \sigma_y}{2}\right) + C. \qquad 1.29$$

This is called the p-q plot where p = $(\sigma_x + \sigma_y)/2$ and q =$(\sigma_y - \sigma_x)/2$. Using this plot, we can graph the direct measured quantities and find the slope and the intersection then converted back to the friction angle and cohesion where

$$\phi = \sin^{-1}(m)\ and \qquad 1.30$$

$$C_o = \frac{C}{cos\phi} = \frac{C}{\sqrt{(1-m^2)}}. \qquad 1.31$$

This model fits most types of rocks at low stress including the ones used in this thesis. However, at high stress, failure point decreases with the increasing radial stress (σ_x). After reaching this limit which is called "Cap", the line starts curve down back to zero. **Figure 1.8** shows that effects after reaching the maximum shear stress (the Cap). In this thesis, we have chosen all the confining stresses such as the sample will not reach the cap and the Mohr-Coulomb failure criteria is valid.

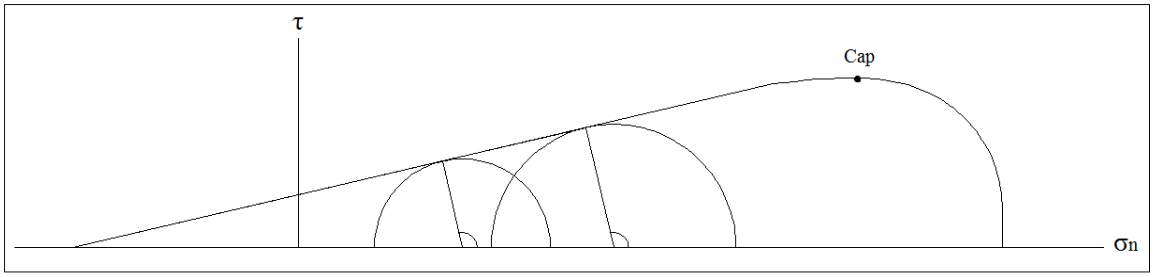

Figure 1.8: The limitation of Mohr-Coulomb model after reaching the Cap stress.

1.1.4 Definition of Deviatoric Stress

As discussed above, the stress that causes failure of the sample is the axial stress minus the radial stress $(\sigma_1 - \sigma_3)$ which is called the deviatoric stress. Therefore, in this work whenever we refer to axial stress we will mean the deviatoric stress the stress which causes failure of the sample.

1.2 Strain

When a sample is loaded as in **Figure 1.9**, it will experience two displacements; one in the axial direction (ΔL), and the other in the radial direction (Δr). The strain is defined as the normalized displacement of the sample to the original length of the sample. Strain is therefore dimensionless, but in most cases lithified samples such as those used in this study occur at 1% to 2%. As a result, to avoid small numbers strain is typically given in milli strains which is the strain multiplied by 1000.

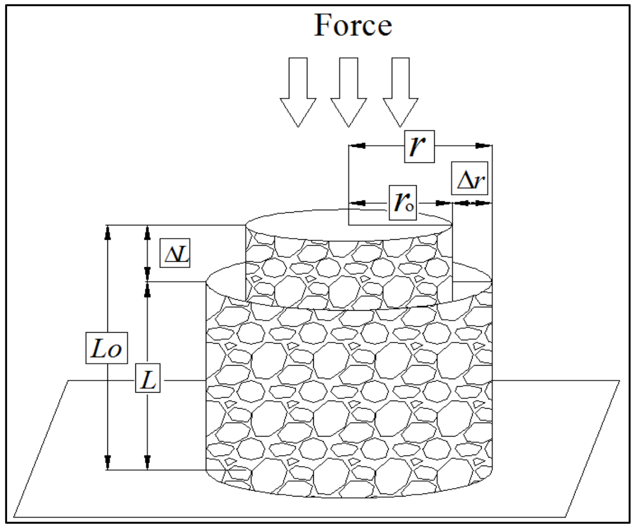

Figure 1.9: Cylindrical rock induced to a certain compressional force.

Given that Lo, r_o are the original length and radius of the sample, then the axial strain is given by the equation

$$\overrightarrow{\epsilon_a} = \frac{\overrightarrow{\Delta L}}{L_o}, \qquad 1.32$$

and the radial strain

$$\overrightarrow{\epsilon_r} = \frac{\overrightarrow{\Delta r}}{r_o}. \qquad 1.33$$

The volume strain can be derived from both the axial and radial strains, it is defined as the change of the volume (ΔV) divided by the original volume (V_o), in other words it is given by the equation

$$\overrightarrow{\epsilon_v} = \frac{\overrightarrow{\Delta V}}{V_o}. \qquad 1.34$$

The volume of the cylinder is $2\pi r^2 L$, and then the change of the volume is given by the equation

$$dV = \left(\frac{\partial V}{\partial L}\right)_{r_o} dL + \left(\frac{\partial V}{\partial L}\right)_{L_o} dr. \qquad 1.35$$

The initial volume of the cylinder is given by

$$V_i = \pi r_i^2 L_i, \qquad 1.36$$

$$dV(r = r_i, L = L_i) = dV_i = \left(\frac{\partial V}{\partial r}\right)_{r_i,L_i} dr + \left(\frac{\partial V}{\partial L}\right)_{r_i,L_i} dL \; and \qquad 1.37$$

$$dV_i = 2\pi r_i L_i \, dr + \pi r_i^2 \, dL. \qquad 1.38$$

The definition of the volume strain is given by

$$\epsilon_v = \frac{dV_i}{V_i}. \qquad 1.39$$

This gives

$$\epsilon_v = \frac{2\pi r_i L_i \, dr}{\pi r_i^2 L_i} + \frac{\pi r_i^2 \, dL}{\pi r_i^2 L_i} = 2\frac{dr}{r_i} + \frac{dL}{L_i}, and \qquad 1.40$$

$$\epsilon_v = 2\epsilon_r + \epsilon_a. \qquad 1.41$$

By definition, the sign of the strain is positive when the sample is compressed (shortened) and negative when the sample dilates (expands). For most of rocks, the change in the length and the diameter is very small related to its original ones when the sample reaches the failure point. Therefore, the expression (1.41) is valid for the entire test. Figure **1.10** shows the volume strain of the sample, we notice that at the beginning the sample volume strain is positive (the sample gets smaller) but after reaching a certain point which is called the positive point of dilatancy, the volume strain becomes negative until reaching the MCS followed by the post failure region.

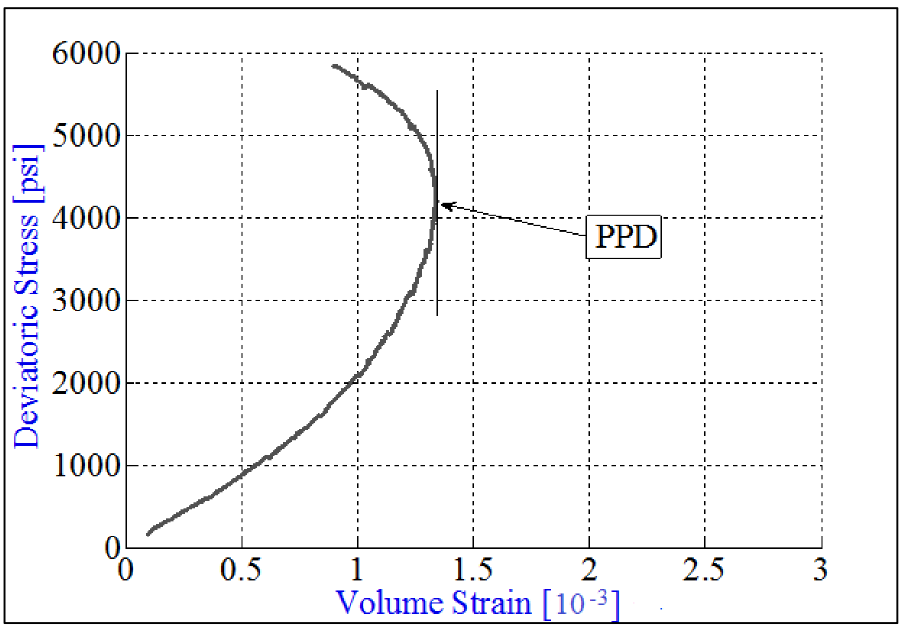

Figure 1.10: An example of point of positive dilatancy (PPD) taken from Single Stage Triaxial test that can be used in Multistage Triaxial test.

1.3 Rock Stiffness and Poisson's Ratio

The rock stiffness can be defined as the change of the stress applied to the sample unit of strain. It represents the resistance of the sample against the stress applied to it, the relation is given by the formula

$$E = \frac{d\sigma}{d\epsilon}. \qquad 1.42$$

This is called the "Young's" modulus (YM) or E-modulus, which is the slope on the stress-strain plot.

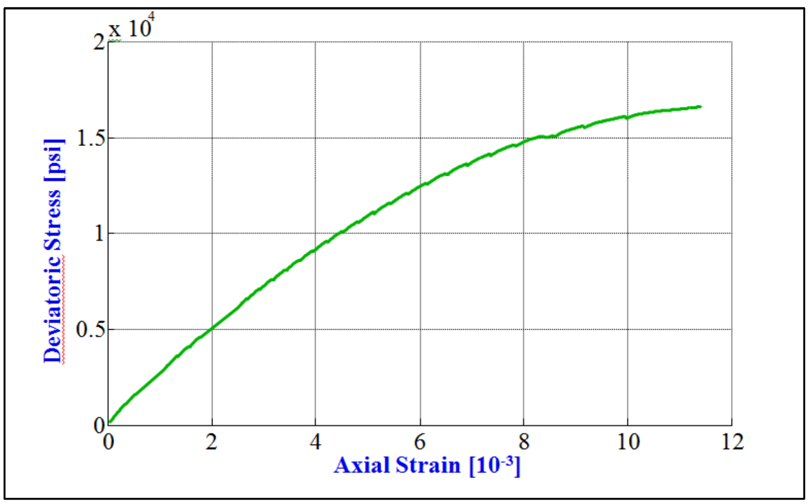

Figure 1.11: A typical stress/strain plot, the slope of this curve is often called Young's modulus. This is strictly true only for elastic materials.

Initially for rocks there is a linear relationship between the applied stress and the resulting strain. In rocks, there is often a linear relationship at low stresses while at high stresses, this relation deviates from the linear behavior and at even higher stress, the reaches to the failure point. **Figure 1.11** shows the behavior of a typical rock sample.

Poisson's Ratio (PR)

When the axial stress is applied to a sample the sample also expands radially. The ratio of the radial strain to the axial strain is called Poisson's ratio and it is given as

$$v = -\frac{d\epsilon_r}{d\epsilon_a}. \qquad 1.43$$

As a result of the negative sign, when (v) is positive, both strains are acting oppositely. In contrast, when (v) is negative, both strains acting the same like in the Uniaxial test when the same compressional stress applied equally to the sample. Therefore, the sample will be compressed radially and axial and both strains are positive. Figure **1.12** shows the Poisson's ratio of a portion of data on the axial/radial strain plot.

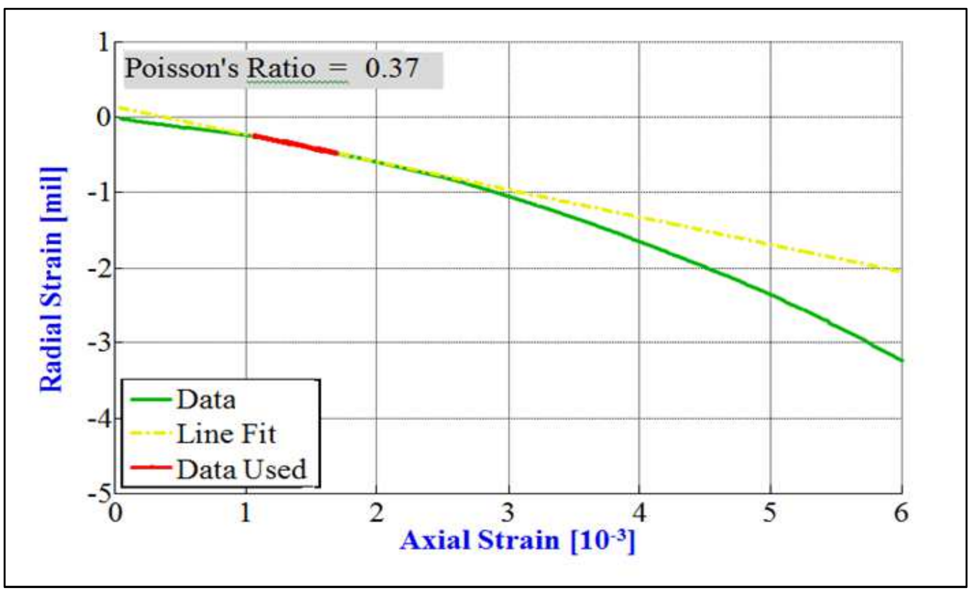

Figure 1.12: Poisson's ratio which is the slope of axial/radial strain plot for a portion of data (red line).

Chapter 2 : Rock Mechanical Tests and Data Evaluation

2.1 Testing Equipment

One inch diameter by two inch long cylindrical rock plugs are used for all the tests in this study. Figure **2.2** shows the triaxial cell used to perform the tests. The pressure vessel is lowered and filled with oil to apply the confining pressure.

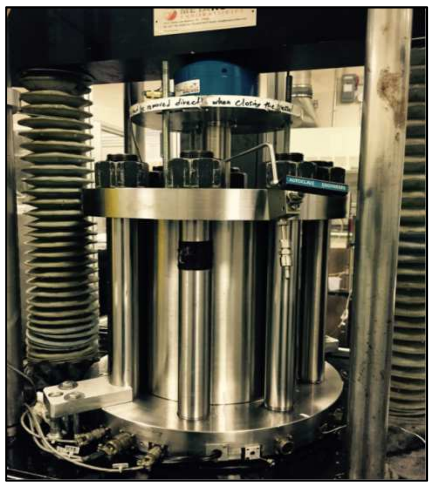

Figure 2.1: The pressure vessel.

The sample is mounted on the bottom of the vessel where it is sleeved between two end caps. The sleeve is typically Viton® that highly elastic but will not rupture at the high confining pressures. **Figure 2.3** shows a drawing of the sample mounted with the end caps.

Figure 2.2: The rock mechanics testing system.

To measure the axial and the radial strains, two LVDTs and one cantilever bridge is mounted with the sample as shown in **Figure 2.3**. The LVDTs are used to measure the axial strain between the endcaps and the cantilever bridge performs a two point measurement of the radial strain. The load cell is mounted in the bottom of the pressure vessel to measure the axial load. Also, acoustics transducers are mounted in the end caps to measure acoustic velocity of the sample.

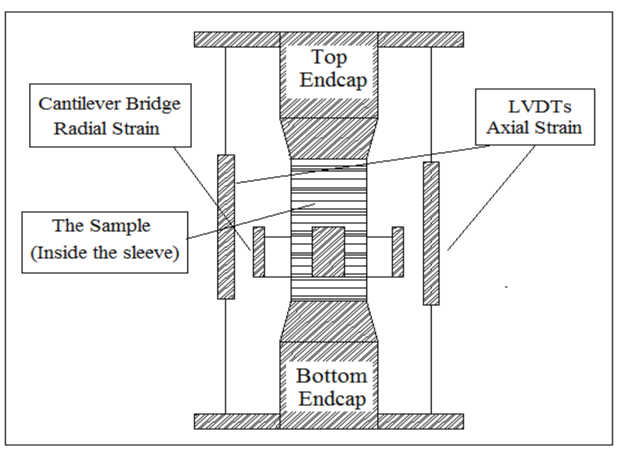

Figure 2.3: The construction of the sample between the end caps that is mounted inside of the vessel with attached transducers for the axial and radial strains measurements.

A graphical user interface (GUI) is used to set up the experiment. Also, it has the ability to make plots for the real time measurements where the user can see the current behavior of the rock under the test. In **Figure 2, 4** we show the main GUI of the system where the pressure vessel top is raised lowered.

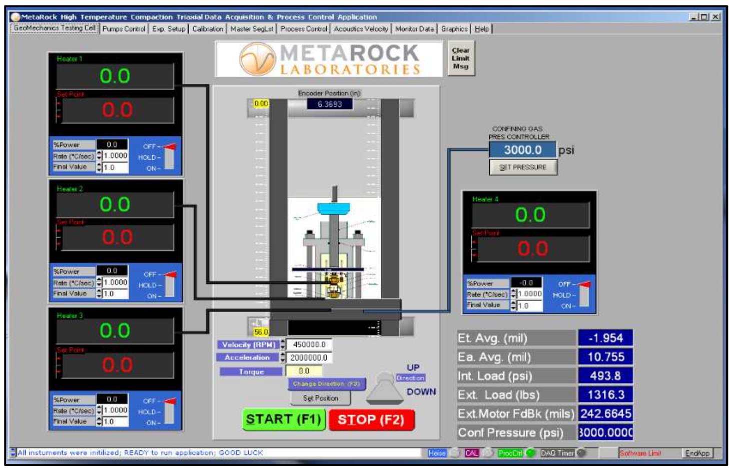

Figure 2.4: The main GUI of the rock mechanical testing that is used to raise the vessel up and down and apply temperature to the test.

One of the most important parts of the GUI is the Master Segment List which is used to set the test routine. Any type of rock mechanical test can be programmed as steps. **Figure 2.5** shows a triaxial test under a confining of 2000psi.

2.2 Triaxial Test Protocols

The two types of triaxial tests compared for this study; single stage triaxial test (SST) and multiple stage triaxial tests (MST). In SST, constant confining stress is applied to the sample while the axial load is increased until the sample reaches the maximum compressive strength (MCS) i.e. until the sample failure. **Figure 2.5** shows one of the SST where a confining stress of 2000psi is applied to the sample, as shown from the figure, the axial load reached the MCS of 16,645psi. The confining stress is shown in green line at 2000psi. Two unloading cycles where applied to the sample to study the magnitude of the recoverable strains.

Figure 2.6 shows the effect of varying the confining stress for “three identical samples” (twins) that were taken from the same depth.

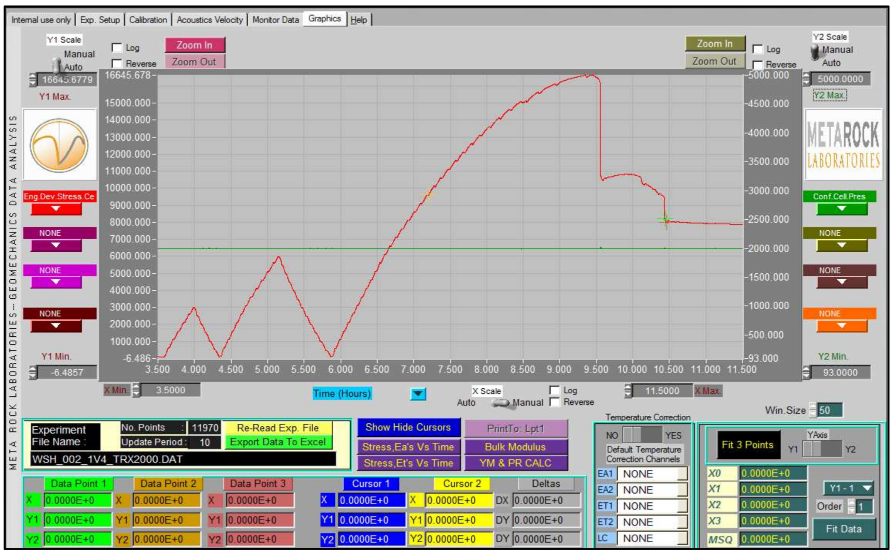

Figure 2.5: SST at 2000psi confining stress.

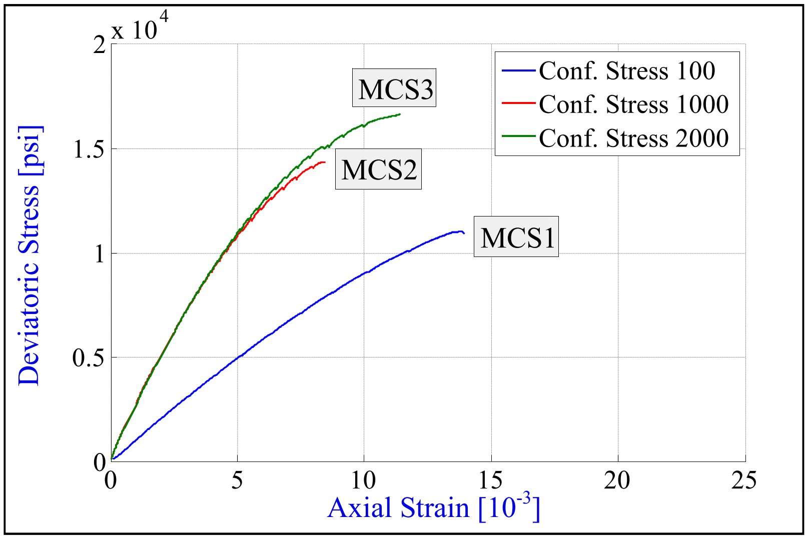

Figure 2.6: The effect of varying the confining stress for a three identical samples where the MCS is proportional to the confining stress.

The MST differs from the conventional tri-axial test in that multiple confining stresses are applied for the same sample as shown in Figure **2.7**. For each confining stage, the axial load is ramped until the point of positive dilatency (PPD) is reached. As discussed above, for the conventional technique, multiple different samples are measured and each is taken to a failure, the maximum compressive strength. Using the point of positive dilatency as the failure criteria minimizes the sample damage at each stage in the multi stage test and provides a unique unambiguous point for comparison. In Figure **2.8** we show an example of using the point of positive dilatency as the failure criterion.

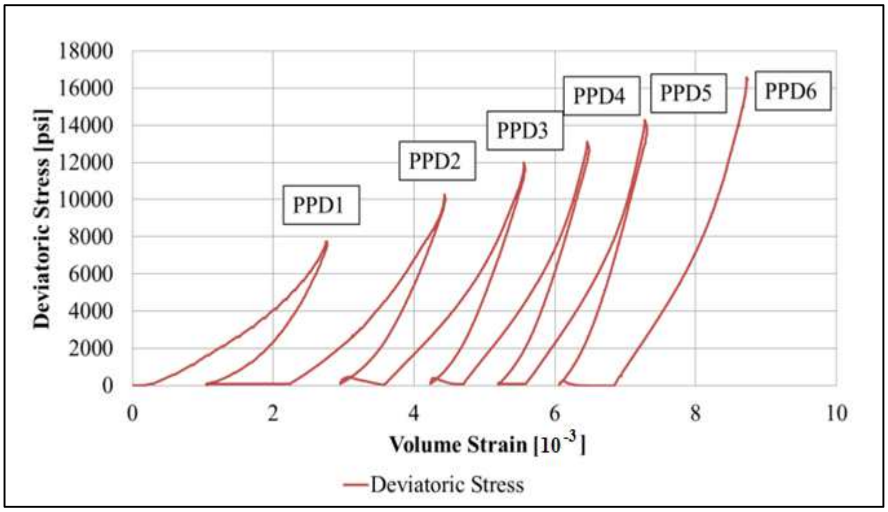

Figure 2.7: MST where different confining stresses are applied to the sample and the axial stress is applied up to the PPD of the sample.

As the slope becomes infinite at PPD, this implies that the change in the volume strain is zero, in other words

$$d\epsilon_v = 0. \tag{2.1}$$

Applying (**2.11.41**) on (**1.41**), it becomes,

$$d\epsilon_v = 2d\epsilon_r + d\epsilon_a = 0, \tag{2.2}$$

$$d\epsilon_v = 2d\epsilon_r + d\epsilon_a = 0 \rightarrow \frac{d\epsilon_r}{d\epsilon_a} = -0.5, and \tag{2.3}$$

$$v = -0.5\,. \tag{2.4}$$

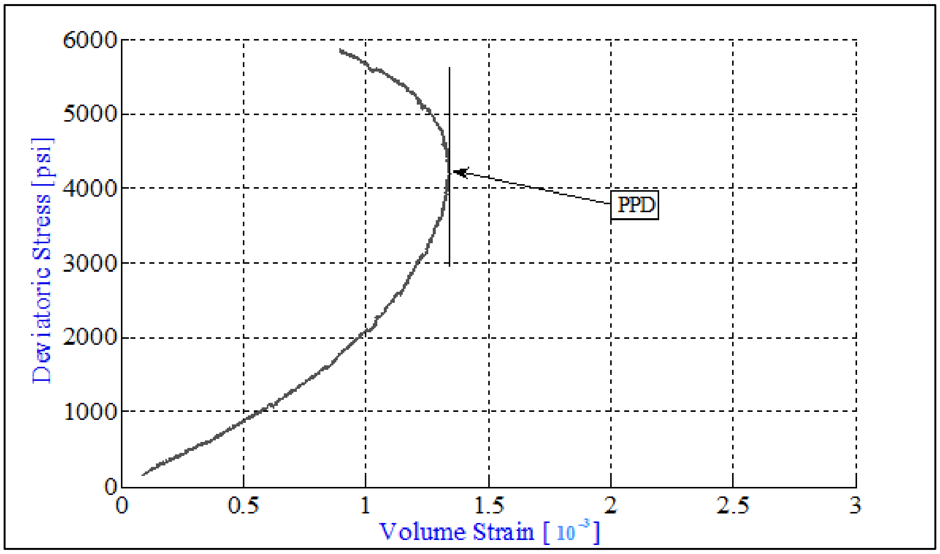

Figure 2.8: PPD criterion that is used in MST which is equivalent to MCS in SST.

At the PPD the Poisson's ratio is **(**0.5**)**, this means that we can equivalently track this point from Poisson's ratio plot. To summarize the MST protocol is performed as the following steps:

1. Apply the initial confining stress.
2. Ramp up the axial stress to the PPD.
3. When reaching PPD, ramp down the axial stress to 100psi and raise the confining stress to the next pressure
4. Repeat steps 1 to 3 until the end of the test.

2.3 Comparing Multistage Test to Single Stage Test

We now compare SST to MST in terms of the main three properties; strength, Young's modulus (YM), and Poisson's ratio (PR). For YM and PR, since YM represents the slope of the axial stress/axial strain plot and PR is the slope of radial strain/axial strain plot which changes with stress. Therefore, a certain window must be defined to find these slopes. For the purpose of this study the PPD is used for both SST and MST to define YM and PR. The slope of the curves between 1/3 of PPD and 2/3 of PPD are reported. **Figure 2.9** & **Figure 2.9** shows an example of the procedure. It is noticeable that the red line in MST is longer than in SST this due to the number of data points that are located within the defined window.

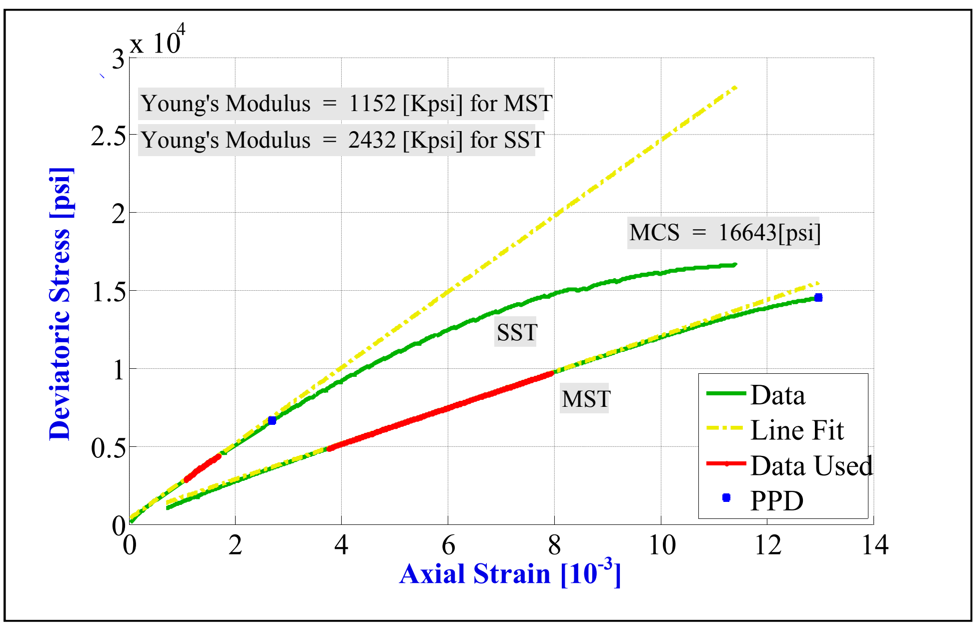

Figure 2.9: YM for SST and MST at a confining stress of 2000psi.

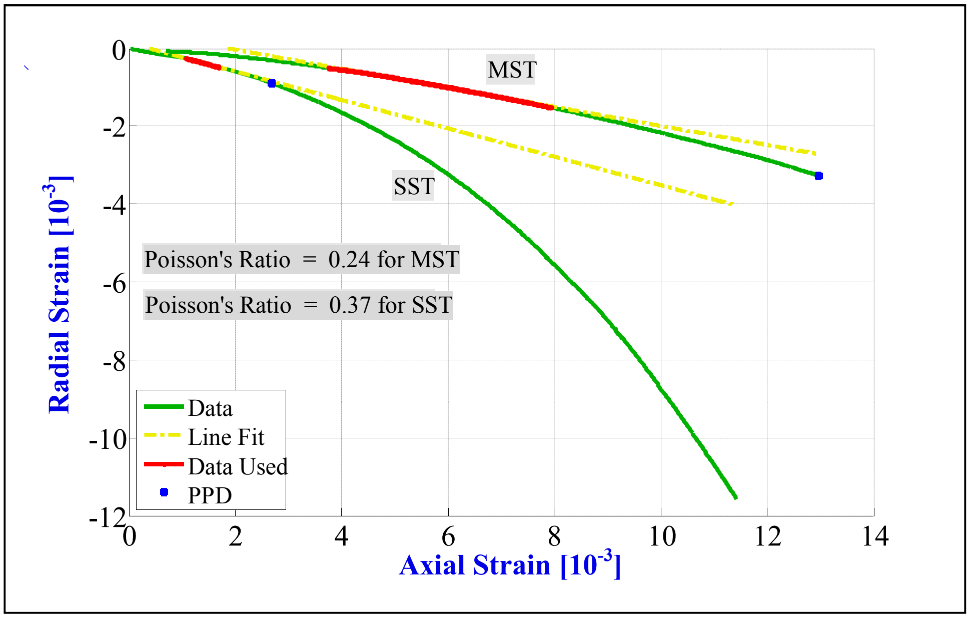

Figure 2.10: PR for SST and MST at same confining stress.

In our study, five types of rock were used. For each type, the basic properties were plot against each other to find the correlation between them if any. In the next chapter we will show the test results for the five types of rocks that were used in this study.

Chapter 3 : Rocks Used, Tests Results and Discussion

For the rock types that are used in this study, we tried to have plugs that have the same properties. As many as five SST were performed on each type of rocks. The confining stresses were chosen to keep the MCS within the linear region where the Mohr-Coulomb model fits and the comparison between SST and MST are still valid. For all tests, cylindrical plugs were used which have dimensions of 1 inch in diameter and 2 inches in length. In this chapter we will provide the test results and the comparison of the main properties.

3.1 Miocene Sandstone

The Miocene sandstone is offshore Louisiana sandstone belongs to the Miocene epoch. These samples were all taken from a depth of ~10,000 ft. **Figure 3.1** shows a plug of this type of rocks.

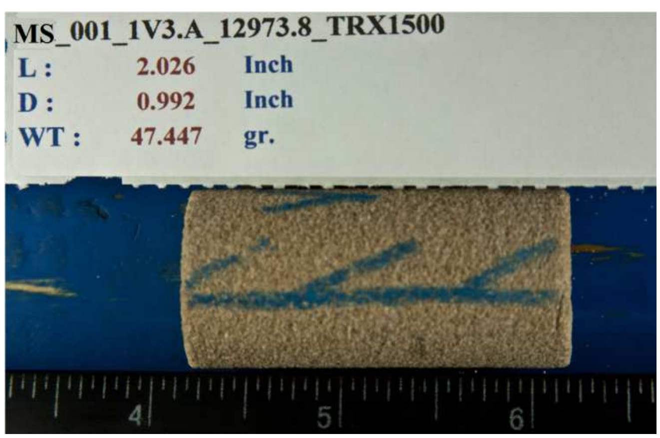

Figure 3.1: Miocene sandstone sample for SST at 1500psi confining stress.

Test Results

Four SST test were performed on the Miocene Sandstone. The upper limit of the confining stress to keep the MCSs within the linear region is found to be below 2200psi. Therefore, we applied the confining up to 1500psi. Figure **3.2** shows one of the SST performed using 500psi confining stress.

Figure 3.2: Triaxial test under confining stress of 500psi as displayed by the real time data acquisition system.

To be consistent with SST, same confining stresses were applied to the sample in MST test. We started with 100psi stress. After reaching the PPD, the confining stress was increased in steps of 500psi until reaching 2200 psi confining stress. Figure **3.3** shows the MST displayed by the data acquisition system where the results are plot vs. time.

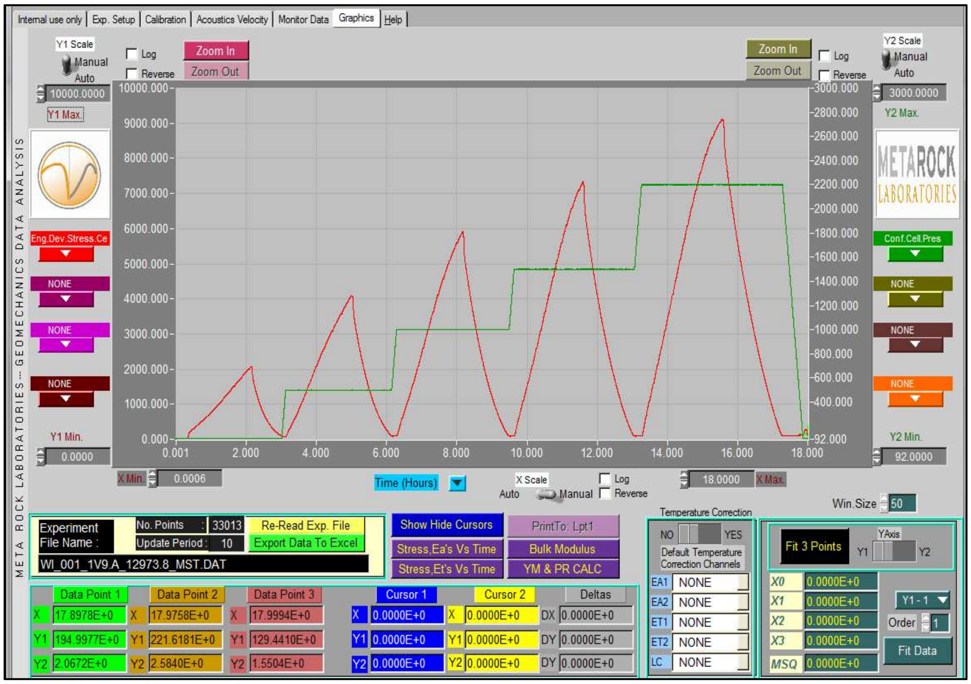

Figure 3.3: The MST test as displayed by the data acquisition system where both confining and the deviatoric stresses are plot against time in hours.

Figure 3.4 shows the plot of the confining and the deviatoric stresses against the volume strain, notice the PPD point where the axial load is decreased to 100psi of deviatoric stress to start the new confining cycle. Also notice the unrecoverable strain when the load is decreased of 50% or less, there is no linear elastic region for this sample. The recoverable strain increases at higher confining stress. There is therefore no evidence of cumulative damage due to the multiple stress cycles applied to the sample.

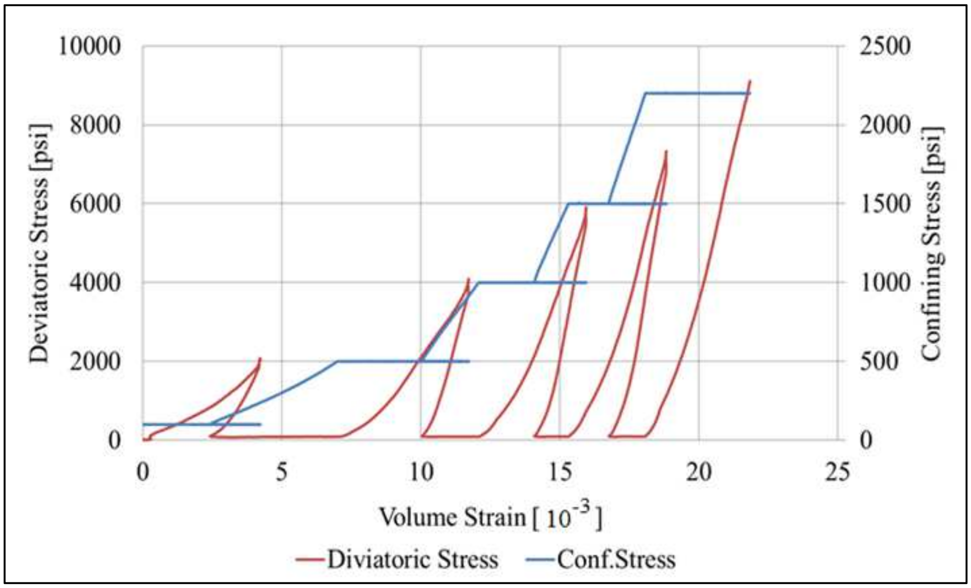

Figure 3.4: The deviatoric and confining stresses that are plot against volume strain.

The summary plot of all the single stage triaxial tests performed on the Miocene is shown in Figure **3.5**. This plot is commonly called fountain plot. We see that the strength of the sample increases as we increase the confining stress. The plot shows clearly that the rock has been reached the cap at 1500psi of confining stress i.e. there is no increase in strength when the confining stress is raised to 2200 psi. Therefore, the two highest MCSs of the sample haven't been used for the correction from MST.

3.1.1 Strength

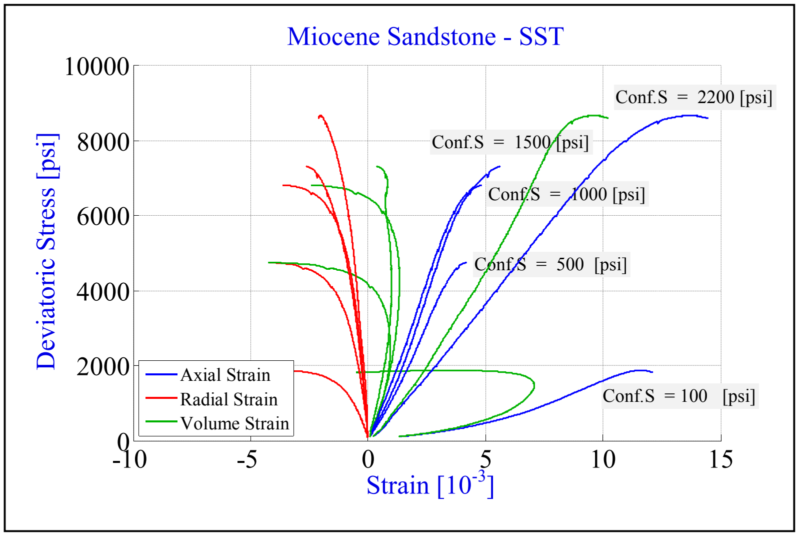

Figure 3.5: The summary (fountain) plot for all the single stage triaxial tests performed on the Miocene sandstone against axial, radial, and volume strains.

Figure **3.6** shows the fountain plot for the MST using the same confining stress applied to SST. However, the PPDs are more consistent even at high stress. However, as discussed above the last two points were not used.

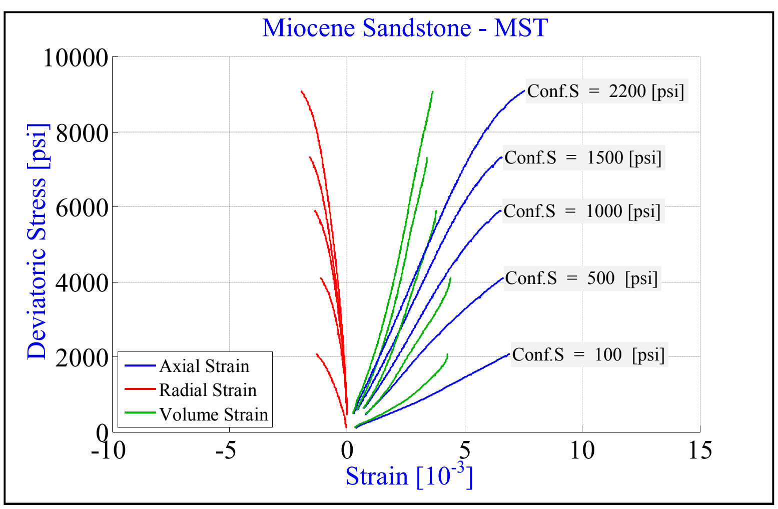

Figure 3.6: The summary (fountain) plot for the multistage triaxial test performed on the Miocene sandstone against axial, radial, and volume strains.

3.1.2 Young's Modulus

Figure 3.7 is a plot of the derivative of the stress strain plots ("Young's Modulus") of the SSTs until reaching the MCSs. As we approach failure, the slope decreases until the MCS is reached. As a rough trend the slope also increases as a function of confining stress. This trend is clearly shown in Figure **3.8** for the MST because of the absence of effects due to sample twinning the trend is much more evident. We will find later that these changes will not affect the correlation between MCS and PPD and the correction still valid between MST and SST.

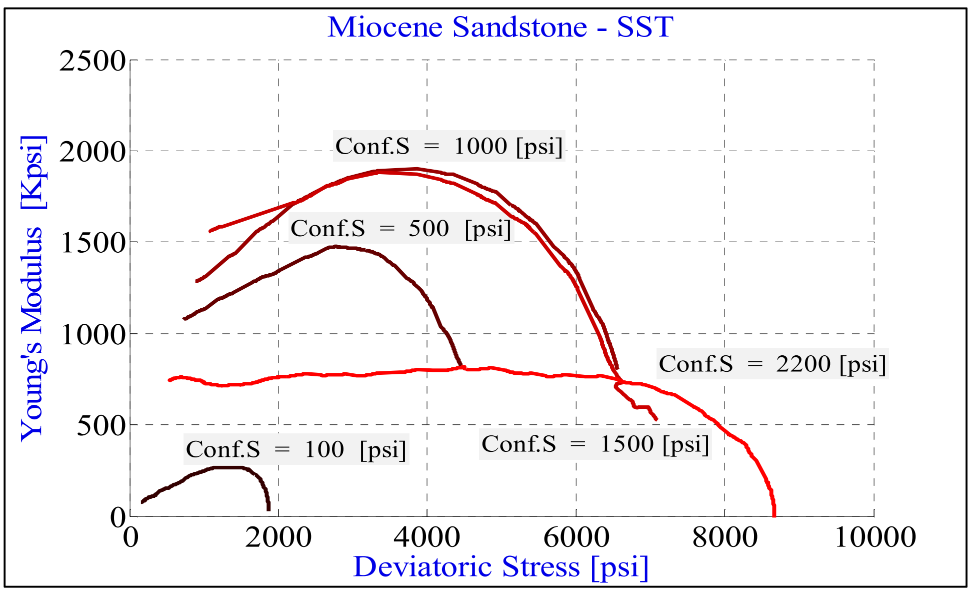

Figure 3.7: The stiffness for all single triaxial tests where it is clear that the stiffness decreases after applying 1500 psi of confining stress.

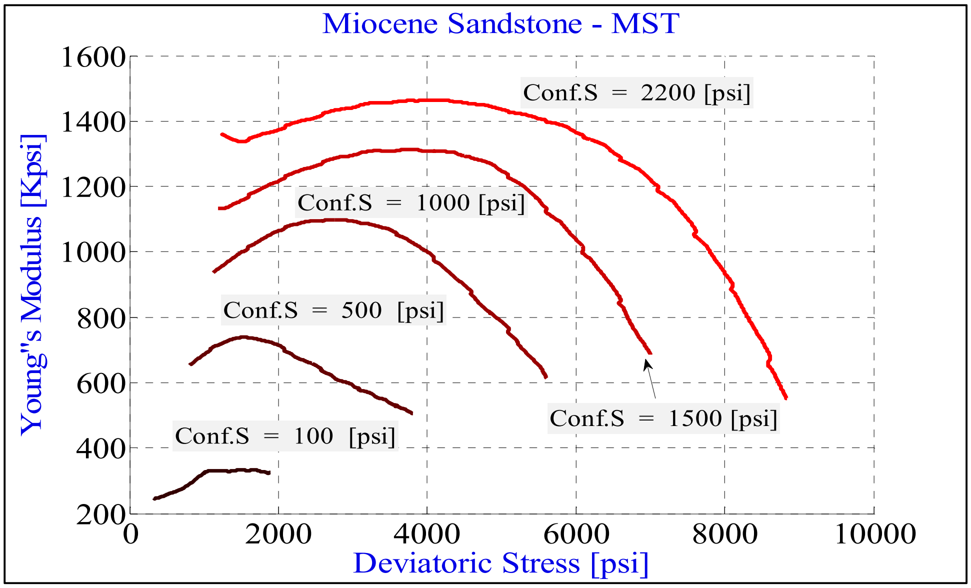

Figure 3.8: The stiffness of the multistage test where the stiffness increases as the confining stress increases.

3.1.3 Results Summary of Miocene Sandstone

Table 3-1 shows summary results for the main three properties related to rock mechanics. The results of the table are plotted to check the correlation between SST and MST in terms of MCS, Young's Modulus (YM), and Poisson's Ratio (PR). The highlighted rows are the points which the Miocene reaches the stress cap and are not used in the correlation.

Table 3-1: Results summary of Miocene Sandstone tests.

Conf. Stress [psi]	SST			MST		
	MCS [psi]	YM [Kpsi]	PR	PPD[psi]	YM [Kpsi]	PR
100	1877	190	0.14	2060	318	0.18
500	4750	1187	0.28	4093	699	0.16
1000	6810	1667	0.25	5907	1089	0.21
1500	7321	1677	0.28	7331	1307	0.25
2200	8670			9110	1447	0.25

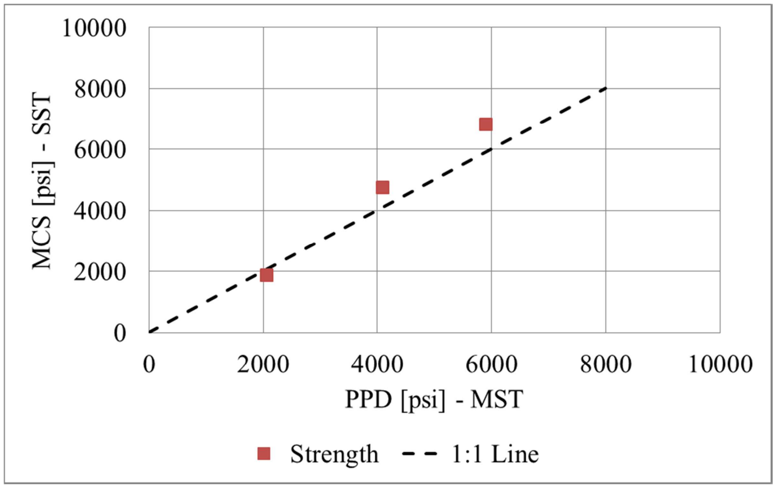

Figure 3.9: Comparison plot of the maximum compressive strength to the point of positive dilatency for Miocene Sandstone.

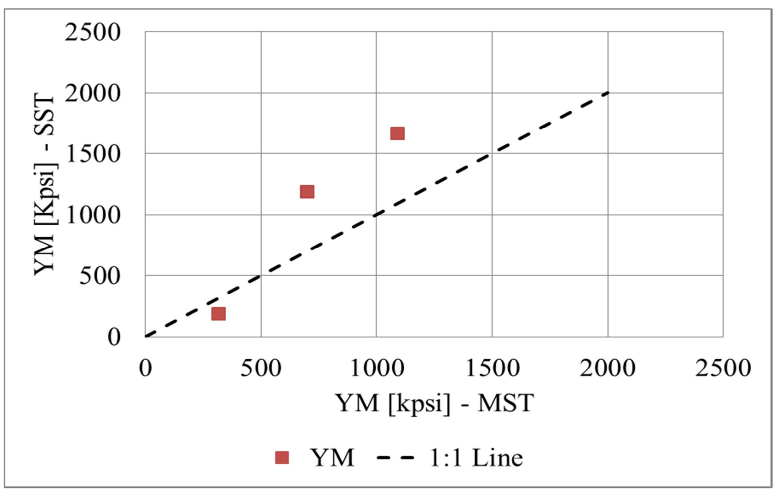

Figure 3.10: Comparison plot of Young's modulus for the Miocene Sandstone.

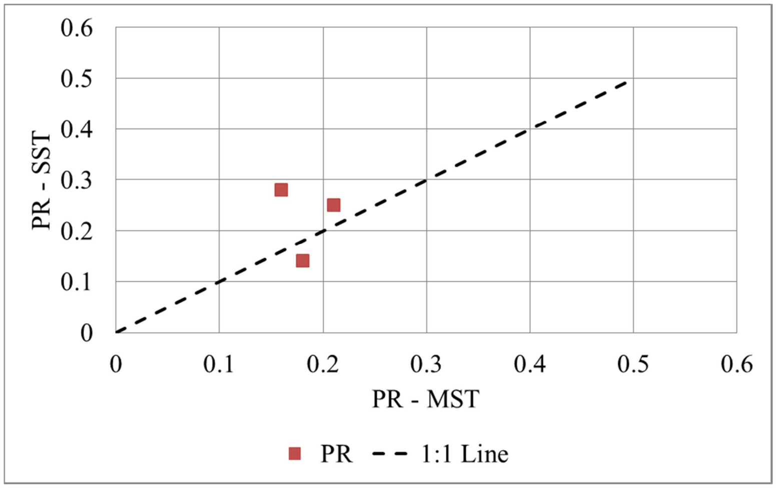

Figure 3.11: Plot for Poisson's ratio for comparing the results of the multi-stage test to the single stage tests for the Miocene Sandstone.

Comparing **Figure 3.9-Figure 3.11**, we observe that the PPD of MST can be corrected to the MCS of SST. However, the correction is more difficult applicable for other properties. We believe that this is due to the sample twinning problem variability in sample selection effect the MCS less than Young's modulus of Poisson's ration. We will find the same situation for the other rock types we studied.

Finally, Figure **3.12** shows the comparison Mohr-Coulomb plot using the failure based on the MCS for the SST and the PPD for the MST. Both exhibit nice linear trends.

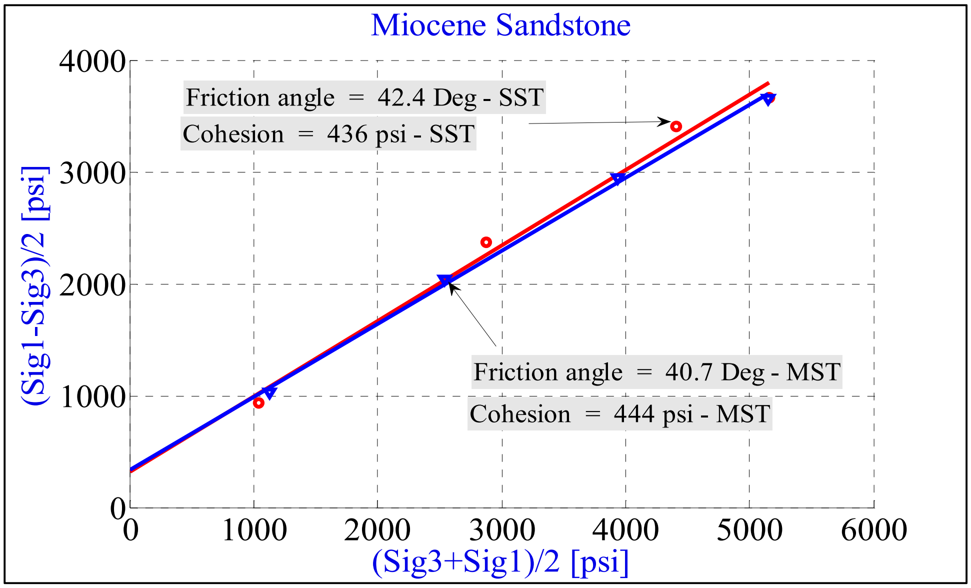

Figure 3.12: Comparison p/q plot of both single stage triaxial test and the multistage triaxial test.

3.2 Woodford Shale

The Woodford Shale Natural Gas Field (Oklahoma Shale) is located in Southeastern Oklahoma. Figure **3.13** shows the location of Woodford Shale in the United States.

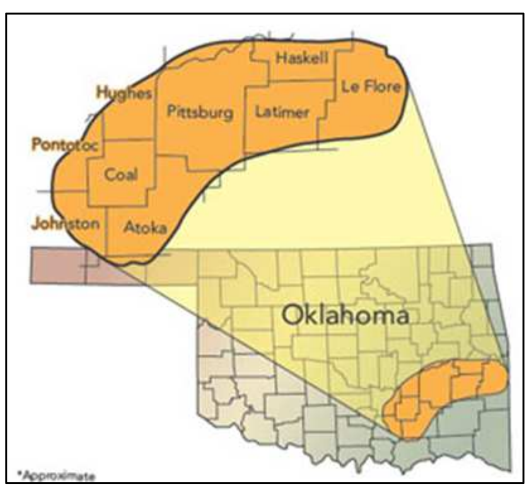

Figure 3.13: The location of Woodford Shale in the United States.

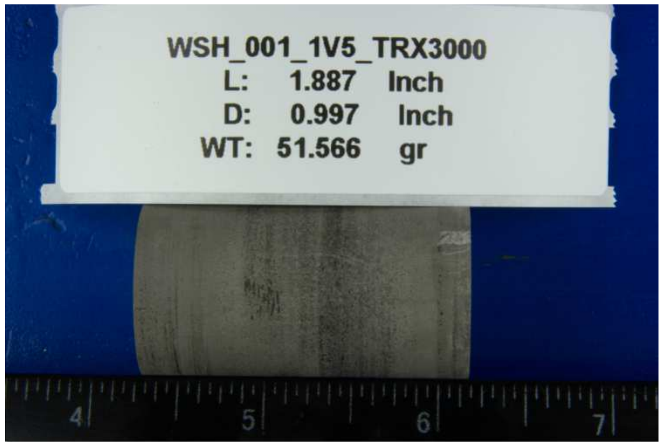

Figure 3.14: Woodford shale sample used for SST at 3000psi confining stress.

Three SSTs were performed on Woodford shale and one MST. The samples were drilled from an outcrop and chosen from as homogeneous region as possible to get samples with similar properties. The confining stresses that were chosen are 100, 2000, and 3000psi and none of the tests shows that the rock reached the cap stress. For the MST, we started from 100psi up to 2000psi in steps of 500psi to have as much data points as possible from a single plug.

Figure 3.15 shows an SST performed on the sample at 2000psi confining stress. The two unload and reload cycles that are shown at the beginning of the test are usually performed to study the recoverable strains and acoustic properties of the rock. Differences were noted between the SST and MST. This analysis will be the subject of future work.

For the MST, we started with 100psi confining up to 2000psi with a 500psi for each step. Figure **3.15** shows the MST evaluated using excel. We can notice the overlapping of the volume strain unloading curve with loading curve this overlapping is due of the large recoverable strains in this material. The recoverable strains were almost 90% which was the largest of any sample measured.

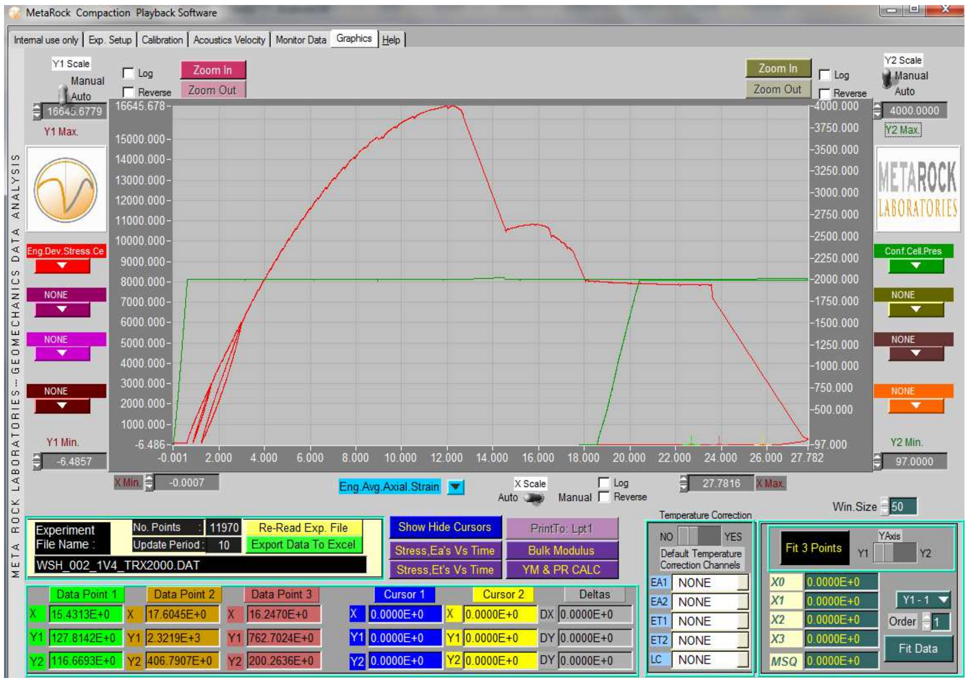

Figure 3.15: Single stage triaxial test is performed at 2000psi confining stress as displayed by the real time data acquisition system.

The same procedure described previously for the loading and unloading was used. We observe that the unrecoverable volume strains are approximately constant for each step and small all consistent with a sample that is dominated by elastic behavior.

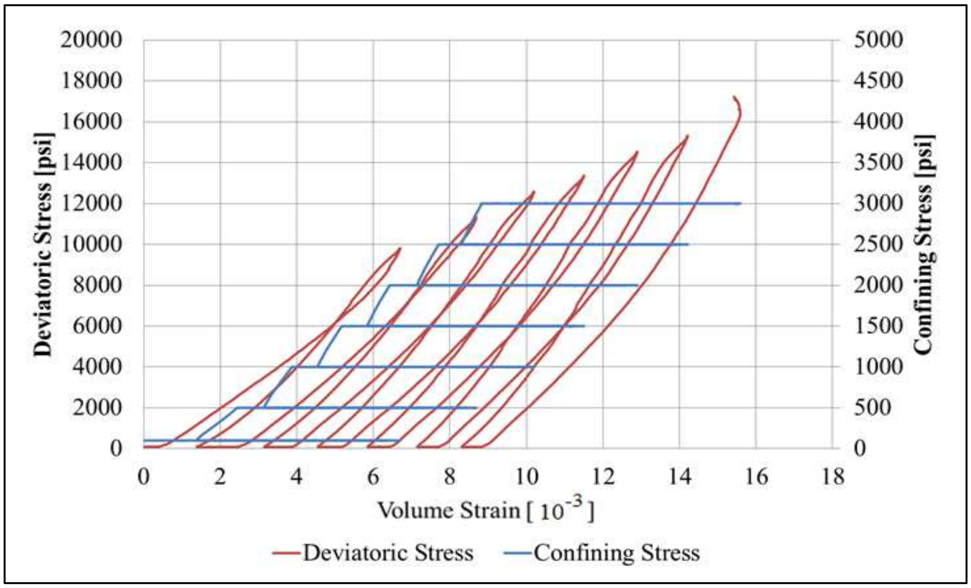

Figure 3.16: The deviatoric and confining stresses that are plot against volume strain.

3.2.1 Strength

The fountain plot in **Figure 3.17** shows the summary of all SSTs performed on the sample. As expected as we increase the confining stress, the MCS increases. However at 3000psi of confining stress, the "Young's" modulus decreases even though the sample fails at a higher stress. This is thought to be due to problems with twinning the sample.

Figure 3.18 shows the fountain plot for the MST. The PPDs show a more consistent behavior with increases in the confining stress i.e. we do not have the sample variation issues.

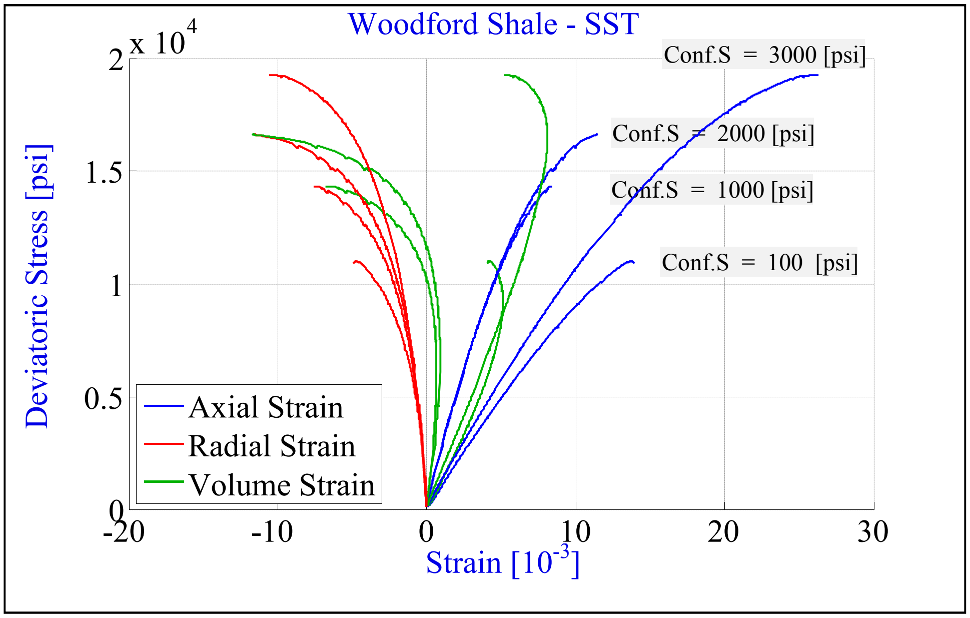

Figure 3.17: The summary (fountain) plot for all the single stage triaxial tests performed on the Woodford shale against axial, radial, and volume strains.

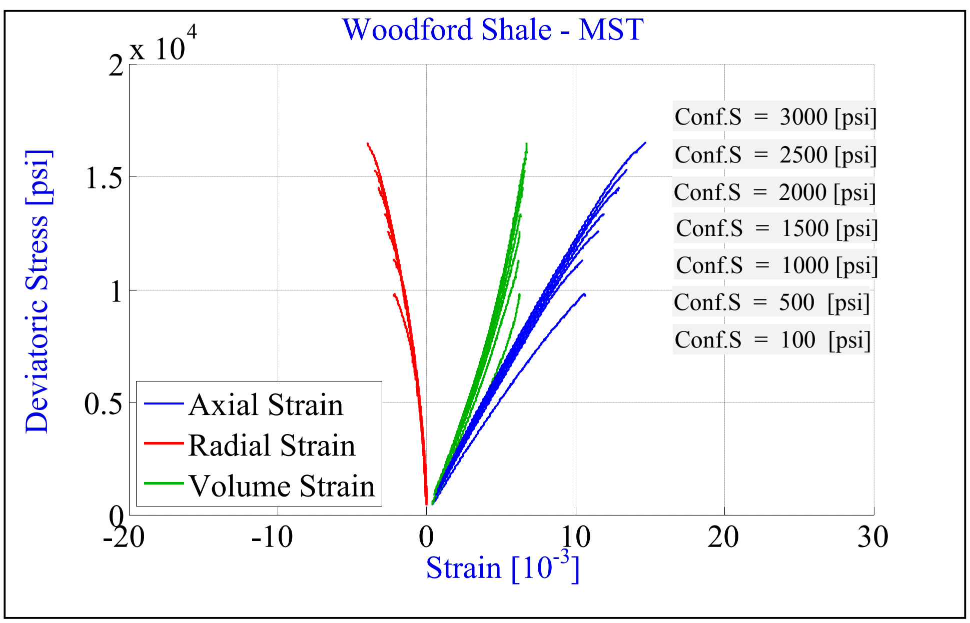

Figure 3.18: The summary (fountain) plot for the multistage triaxial test performed on the Woodford shale against axial, radial, and volume strains.

3.2.2 Young's Modulus

Figure 3.19 shows the slopes of the stress strain plots. The slope increases as we increase the confining stress except at 3000psi confining stress, where the slope is reduced to around 1000Kpsi. This is due to the high confining stress that weakens the sample.

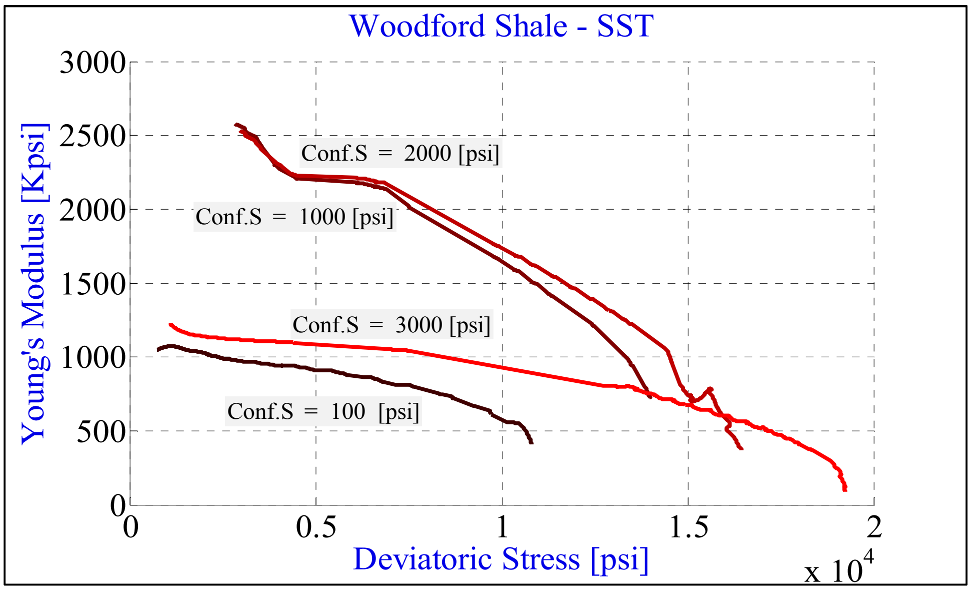

Figure 3.19: The stiffness for all single triaxial tests where it is clear that the stiffness decreases after applying 1500psi of confining stress.

For the MST we see that the stiffness is always proportional to the confining stress. For confining stresses between 500psi to 3000psi there is a slight increase in the stiffness. Therefore, we can consider that as the stiffness remains constant for the MST. Also, it is noticeable that the "nee" point of the curves where the stiffness starts decreasing as we reach the PPD is proportional to the confining stresses between 500psi to 3000psi.

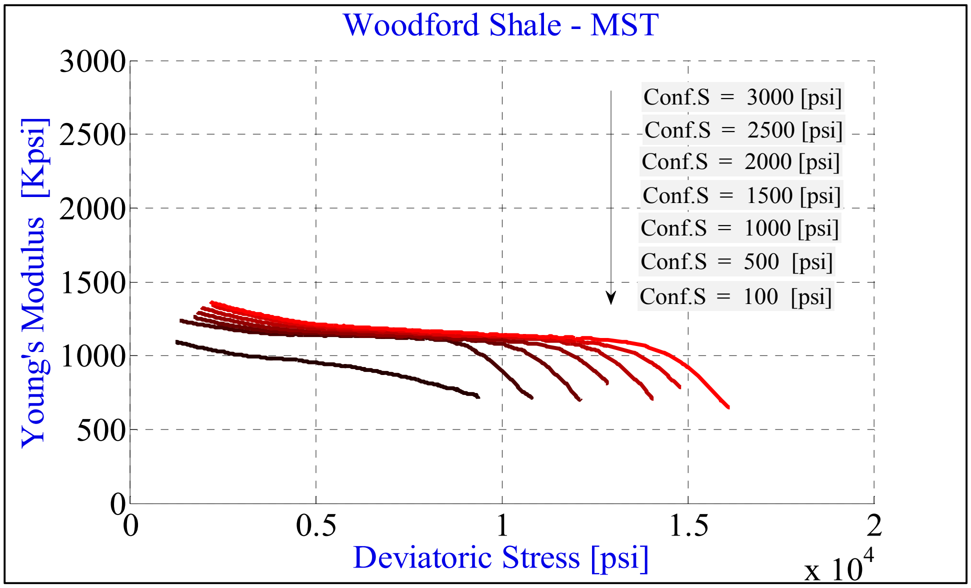

Figure 3.20: The slope of the multistage test shows a small increase with confining stress and is nearly independent of the axial load until failure.

3.2.3 Results Summary of Woodford Shale

Table 3-1 shows the results summary for both SST and MST for the main three properties related to rock mechanics. The highlighted rows show that the results are not available.

Table 3-2: Results summary of Woodford Shale tests.

Conf. Stress [psi]	SST			MST		
	MCS [psi]	YM [Kpsi]	PR	PPD [psi]	YM [Kpsi]	PR
100	11022	932	0.21	9813	955	0.17
500				11317	1134	0.19
1000	14348	2480	0.37	12586	1136	0.22
1500				13363	1140	0.23
2000	16643	2432	0.37	14540	1152	0.24
2500				15322	1157	0.25
3000	19307	966	0.23	16540	1161	0.27

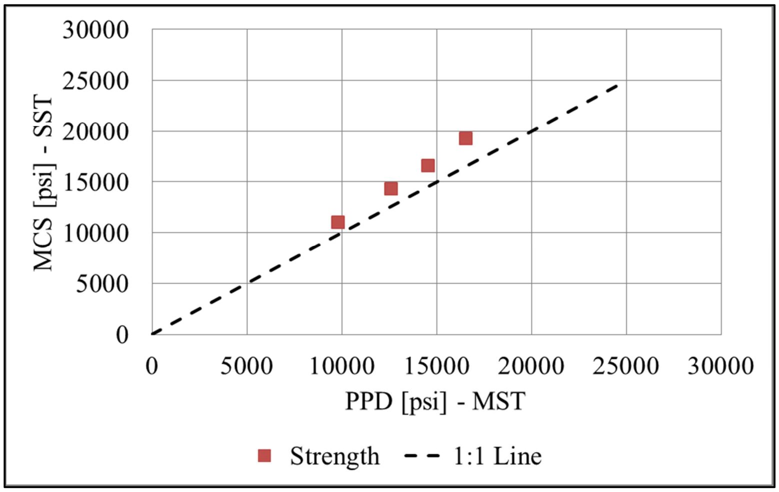

Figure 3.21: Comparison plot of the maximum compressive strength to the point of positive dilatency for Woodford Shale.

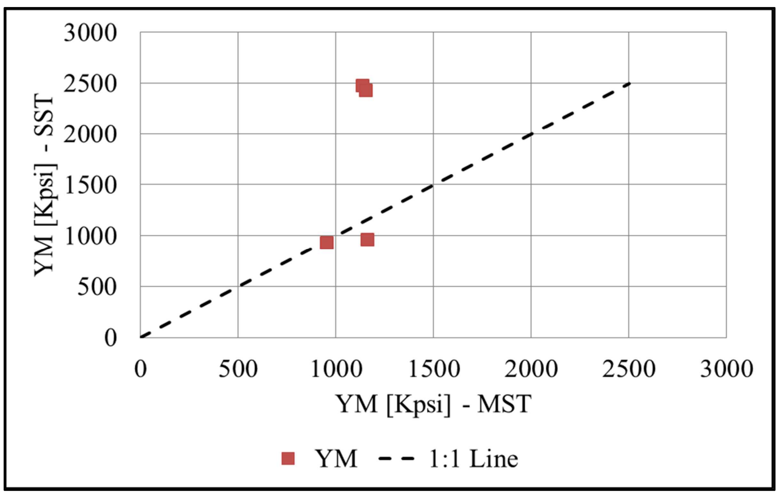

Figure 3.22: Comparison plot of Young's modulus for the Woodford Shale.

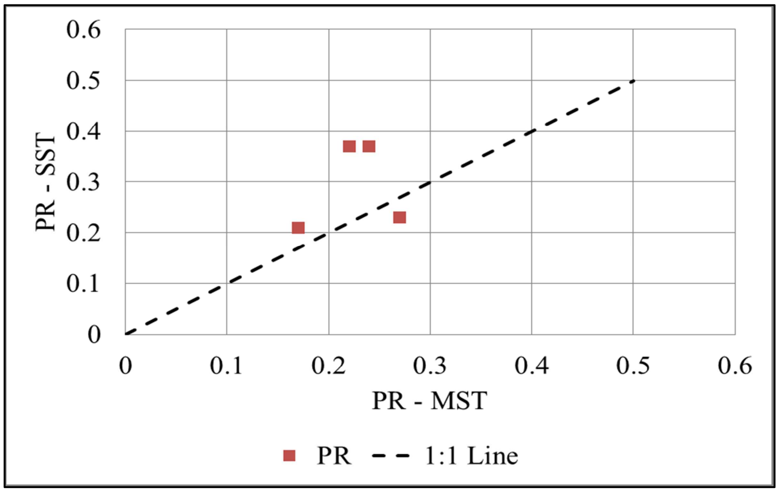

Figure 3.23: Plot for Poisson's ratio for comparing the results of the multistage test to the single stage tests for the Woodford Shale.

We see from Figure 3.25 and Table **3-2** that strength of the MST is highly correlated to SST. However, there is no correlation for both YM and PR. Finally, **Figure 3.24** shows the comparison Mohr-Coulomb plot of both SST and MST for the Woodford shale.

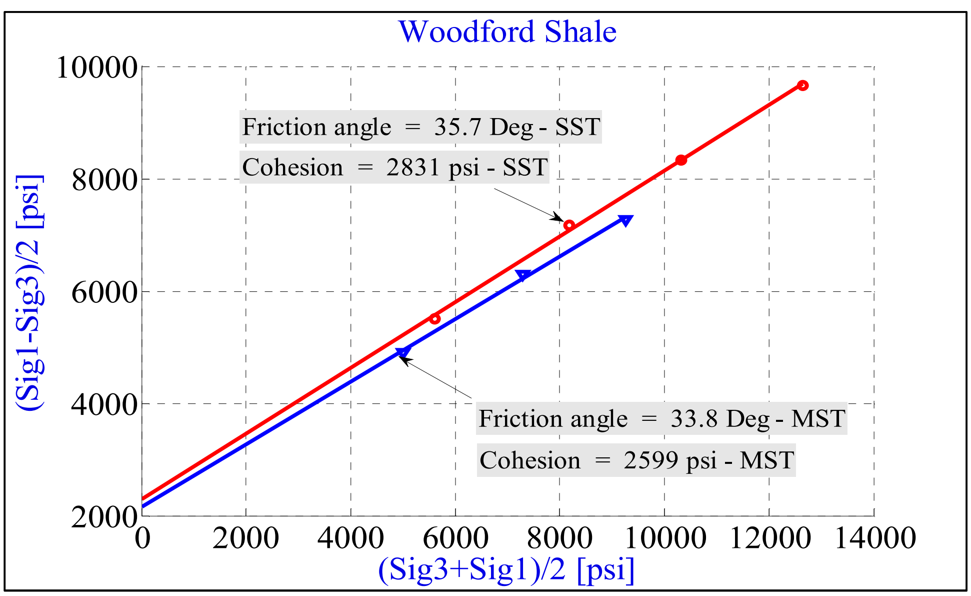

Figure 3.24: Comparison p/q plot of both single stage triaxial test and the multistage triaxial test.

3.3 Mancos Shale

The Mancos Shale or Mancos Group is an Upper Cretaceous geologic formation of the Western United States dominated by mudrock that accumulated in offshore and marine environments of the Cretaceous North American Inland Sea.

The Mancos Shale samples were drilled from outcrop rock. Six SSTs and one MST were performed. For the SST the confining stresses were chosen are from 0psi to 3000psi, and for MST the multiple stages were from 100psi to 3000psi with 500psi increment.

Figure 3.25: Mancos Shale samples.

Figure 3.26 shows a typical SST performed on the sample at 500 confining stress. The two unload and reload cycles that are shown at the beginning of the test are usually performed to measure the elastic properties. For the MST, we started with 100psi confining up to 3000psi with a 500psi for each step. **Figure 3.27** shows the MST. The overlapping of the volume strain unloading curve with loading curve is again evident in the cycles 4 and 5.

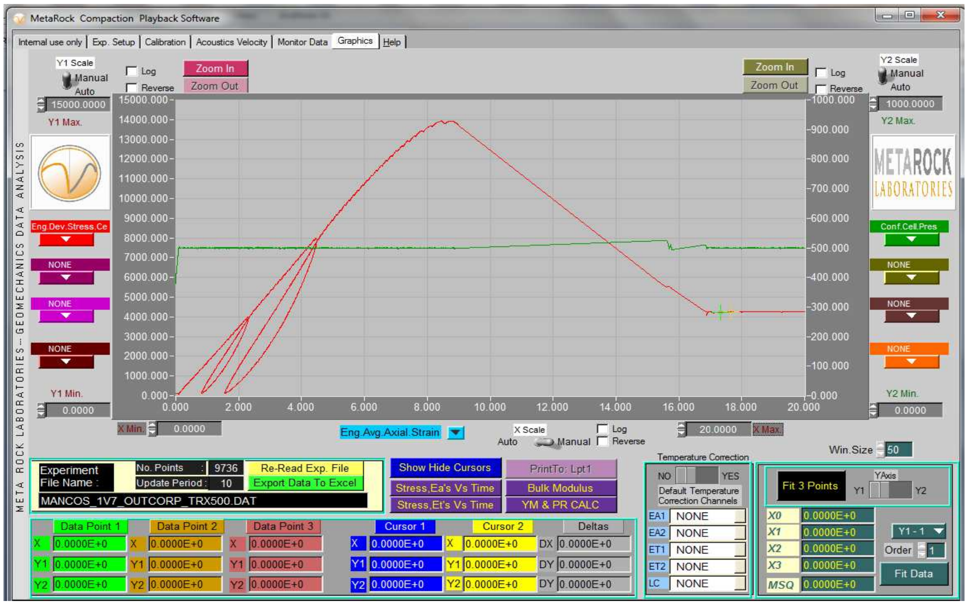

Figure 3.26: Single stage triaxial test is performed at 500psi confining stress as displayed by the real time data acquisition system.

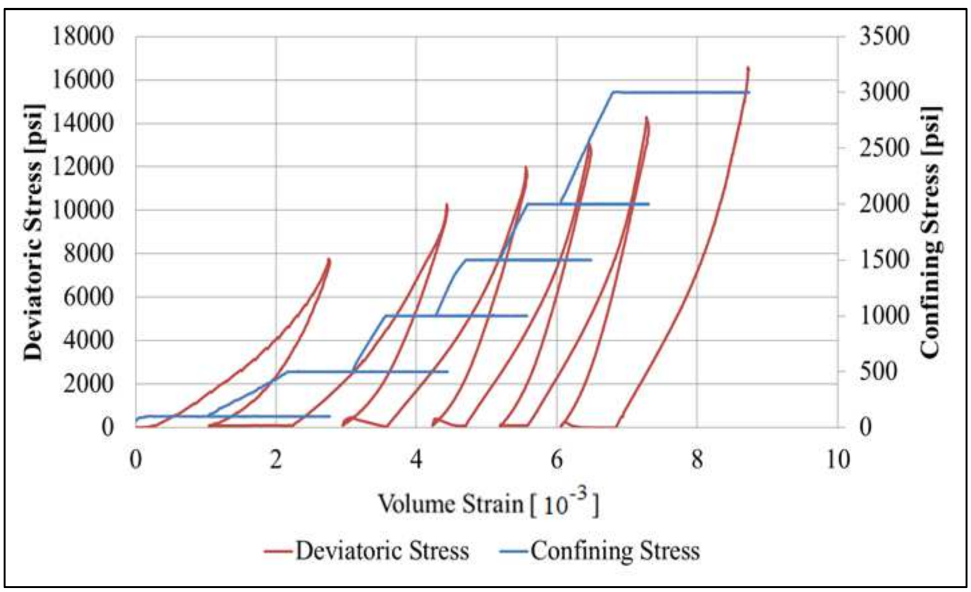

Figure 3.27: The deviatoric and confining stresses that are plot against volume strain.

3.3.1 Strength

Figure 3.28 shows the fountain plot of the SST. The slope of the stress strain curve again depends on the confining stress except for the highest confining stress . This is again attributed to sample variability.

This reversal in the slope of the stress-strain plot does not occur for the MST (**Figure 3.29**). Again, this indicates the import role that sample twinning plays.

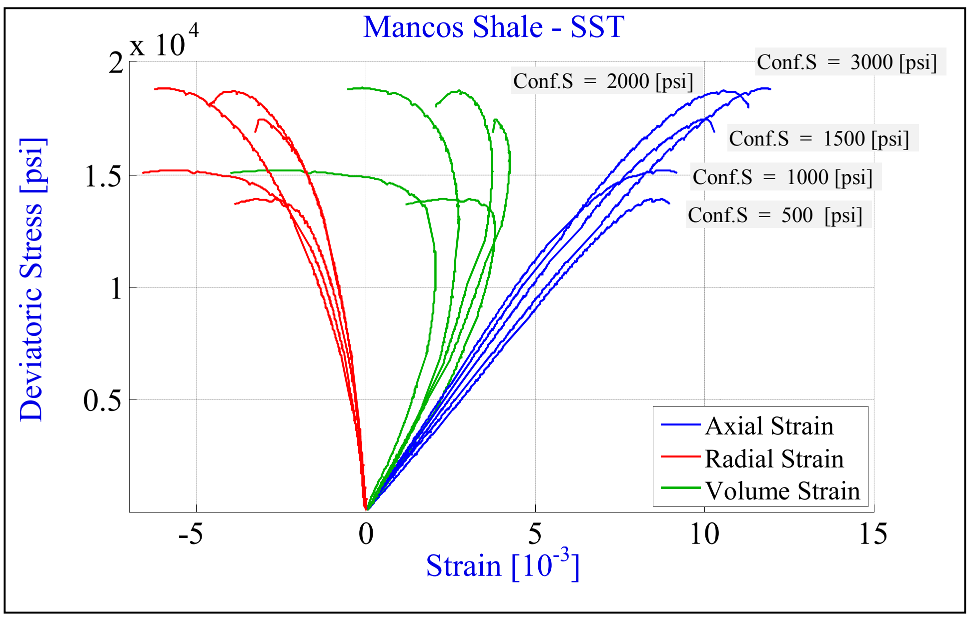

Figure 3.28: The fountain plot of all the single stage triaxial tests performed on the Mancos Shale against axial, radial, and volume strains.

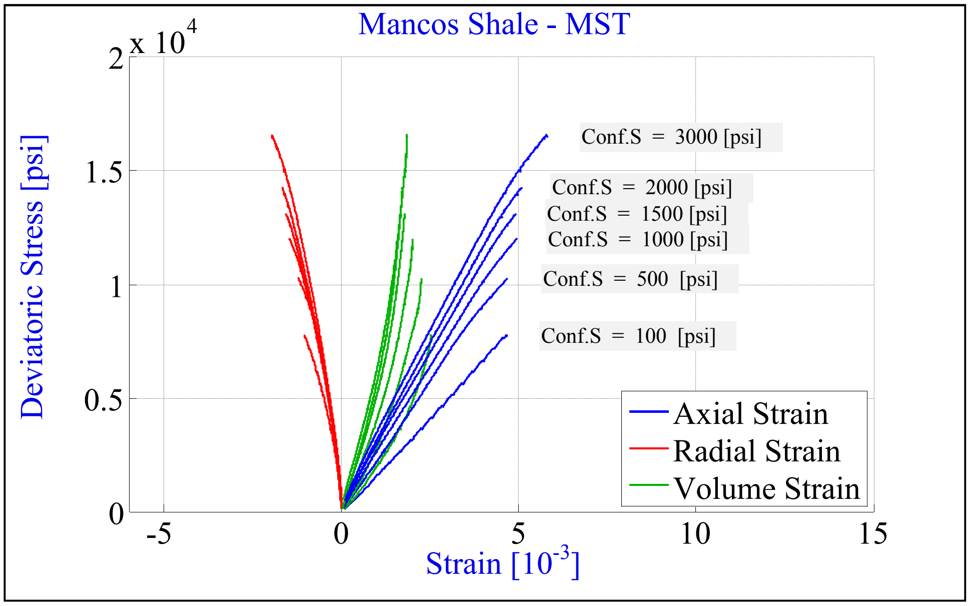

Figure 3.29: The fountain plot of the multistage triaxial test performed on the Woodford shale against axial, radial, and volume strains.

3.3.2 Young's Modulus

For the slope of the stress-strain plots we can see for the SST that the curves cross each other, but as observed above as we increase the confining stress more than the MCSs are still increasing. For the MST, we see the same behavior but with much more consistent trends as shown in **Figure 3.31** where similar behavior to Woodford Shale can be seen as PPDs are more consistent with the increase in the confining stress. This means that we do not have the sample variation issues.

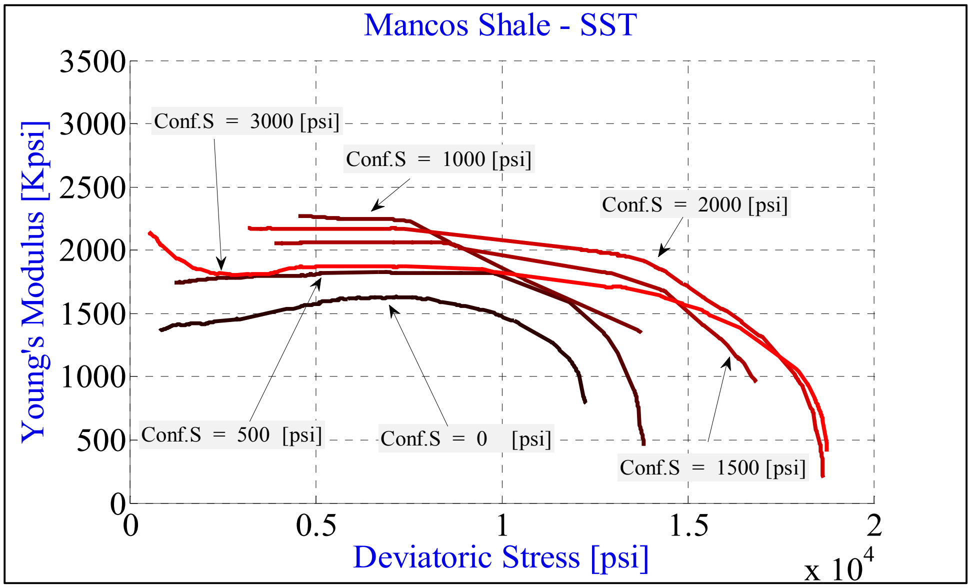

Figure 3.30: The stiffness for all single triaxial tests where it is clear that the stiffness decreases after applying 1500 psi of confining stress.

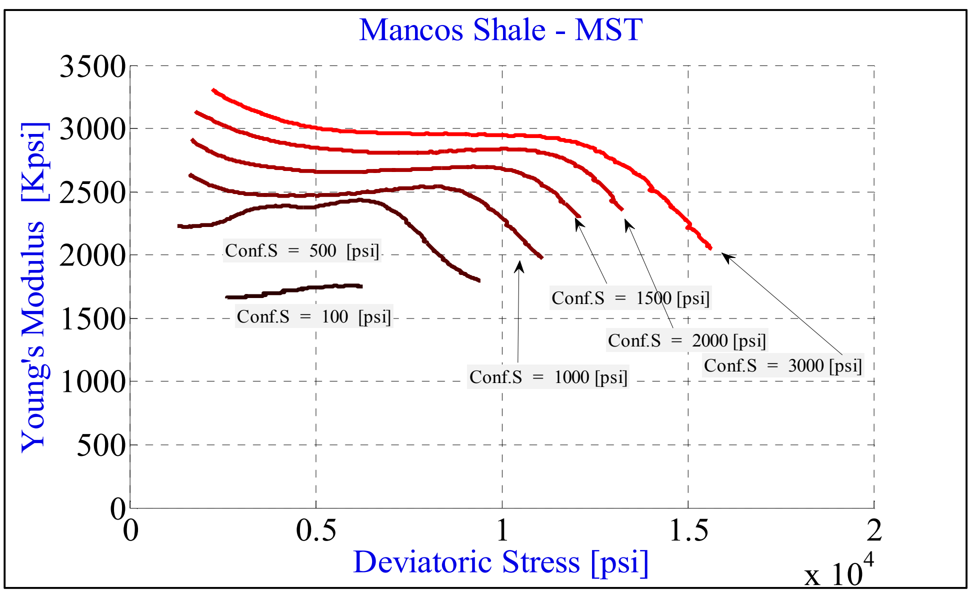

Figure 3.31: The stiffness of the multistage test where it increases as the confining stress increases.

3.3.3 Results Summary of Mancos Shale

The main rock's properties are shown in **Table 3-3** where the highlighted cells are the values that are not used in the data evaluation as the rock reaches the cap pressure. The four tests related to the confining from 500psi to 2000psi are used in the evaluation. We can notice that at 3000psi the MCS which is (18,864 psi) is slightly higher than the MCS (18,739 psi) in the previous stage.

Table 3-3: Results summary of Mancos Shale tests.

Conf. Stress [psi]	SST			MST		
	MCS [psi]	YM [Kpsi]	PR	PPD[psi]	YM[Kpsi]	PR
0	12550	1560	0.21			
100				7754	1701	0.23
500	13938	1867	0.21	10280	2396	0.26
1000	15202	2272	0.25	12000	2490	0.3
1500	17473	2065	0.24	13120	2664	0.32
2000	18739	2172	0.28	14280	2814	0.33
3000	18864	1869	0.3	16580	2956	0.34

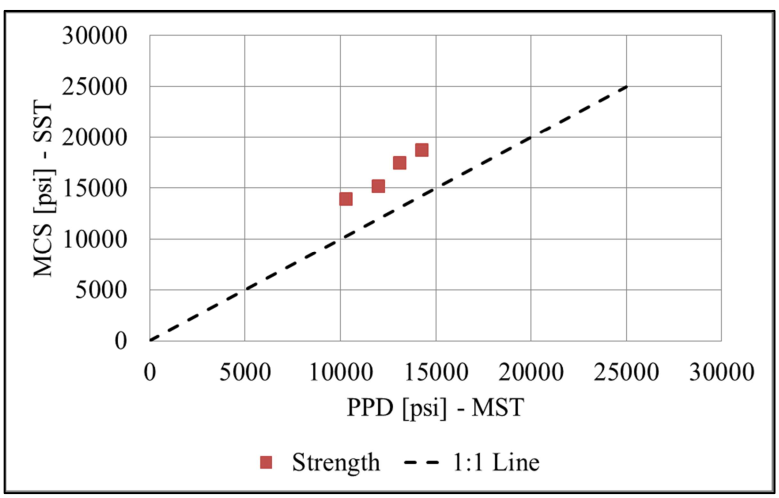

Figure 3.32: Comparison plot of the maximum compressive strength to the point of positive dilatency for Woodford Shale.

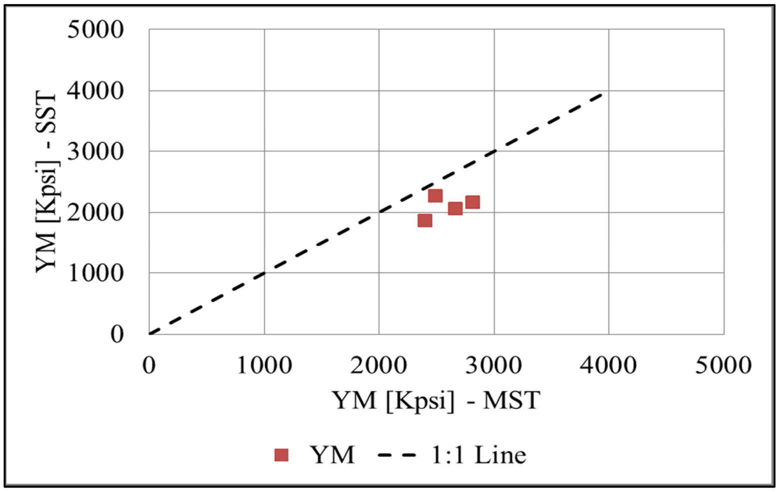

Figure 3.33: Comparison plot of Young's modulus for the Woodford Shale where the stiffness is slightly depends on the confining stress.

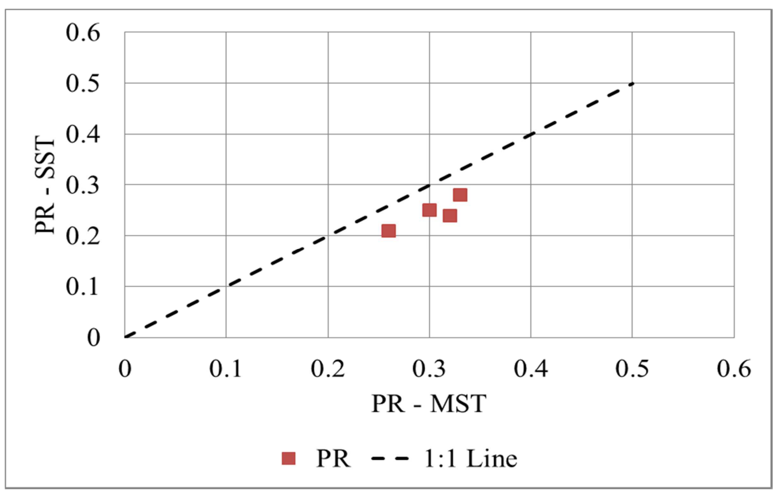

Figure 3.34: Plot for Poisson's ratio for comparing the results of the multi-stage test to the single stage tests for the Woodford Shale.

From Figures **Figure** 3.32 to **Figure** 3.34, we see that a correlation can be found for all the properties between the SST and the MST results. We believe that to be due to the relatively uniform nature of the sample horizon. Finally, the following plot shows the comparison between SST and MST on the p/q plot where similar to previous type of the rocks as the MST has lower values than the SST.

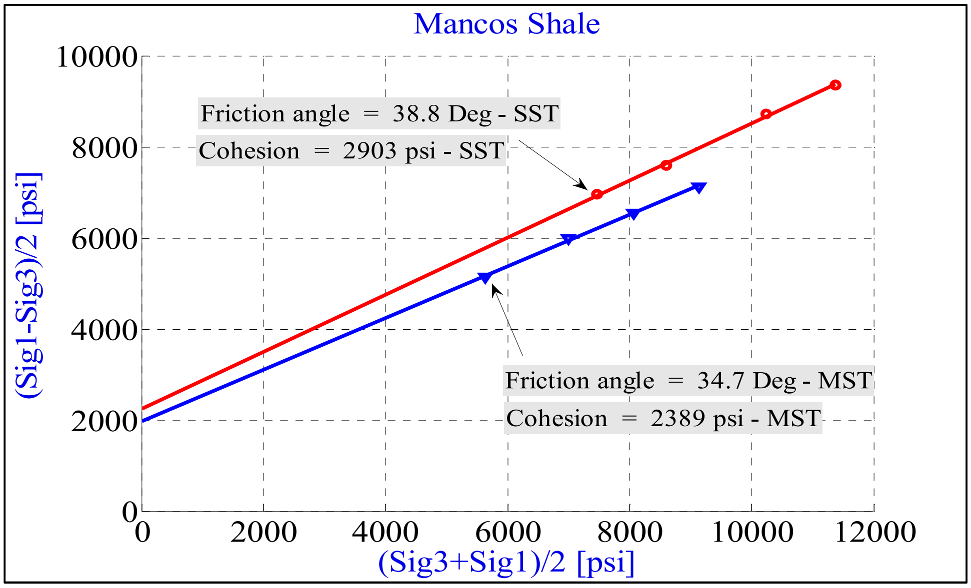

Figure 3.35: Comparison p/q plot of both single stage triaxial test and the multistage triaxial test.

3.4 Austin Chalk

The Austin Chalk is an upper Cretaceous geologic formation in the Gulf Coast region of the United States. It is named after type section outcrops near Austin, Texas. The Austin Chalk consists of recrystallized, fossiliferous, interbedded chalks and marls. Exposures of Austin Chalk are mainly seen in quarries, roadcuts, and stream beds where the water eroded the soil. The Austin Chalk outcrops and can be seen throughout Dallas, and extends south underneath I-35 down into Austin and San Antonio as shown in **Figure 3.36**.

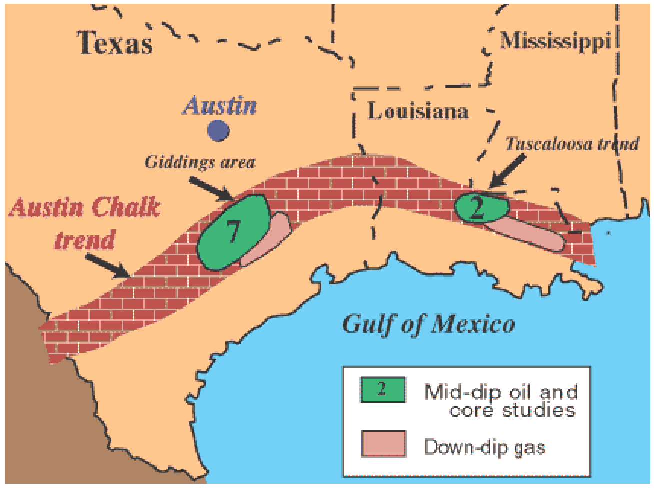

Figure 3.36: The Austin Chalk trend in the United States.

Six SSTs were performed on Austin Chalk and one MST. The samples were drilled from the same outcrop rock to ensure that the plugs have the same properties. **Figure 3.37** shows one plug used in the test. The confining stresses that were used are from 100 to 2000 psi for both SST and MST. None of the tests indicated that the rock reached the cap stress.

Figure 3.37: Austin Chalk sample.

The same procedures were performed for the SST where two unloading reloading cycles are applied to the sample and then we bring it to the MCS point. For the MST, the stress was similar to those described earlier. **Figure 3.38** shows one SST example at 1000psi confining stress.

Figure 3.38: Single stage triaxial test is performed at 1000psi confining stress as displayed by the real time data acquisition system.

For the MST, **Figure 3.39** shows the graph of the test where the deviatoric and the confining stresses is plotted against the volume strain. There is significant irrecoverable volume stain at each reloading and loading cycles but they do not overlap as we observed in the previous two types of the rocks.

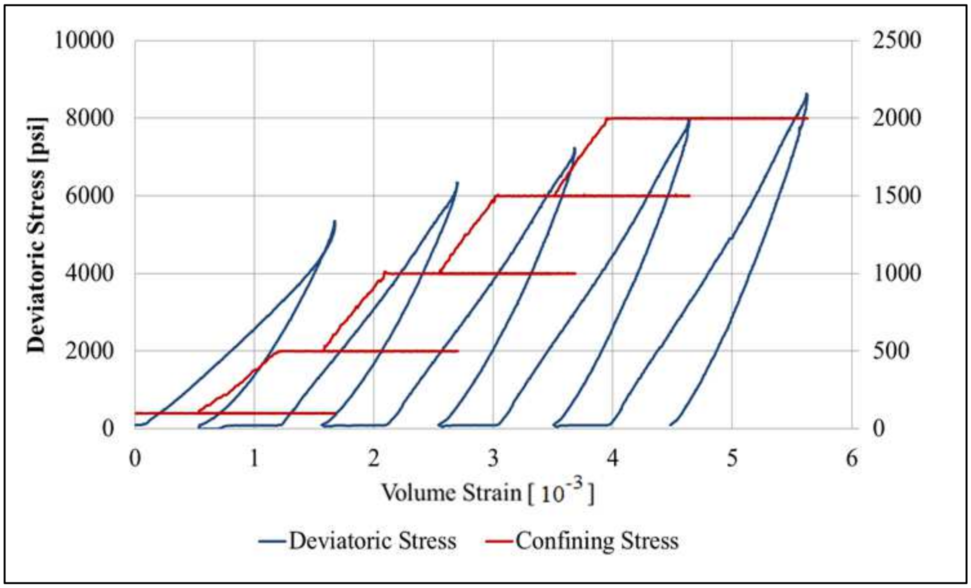

Figure 3.39: The deviatoric and confining stresses that are plot against volume strain.

3.4.1 Strength

The SST fountain plot is shown in **Figure 3.40**, again as we increase the confining stress, the MCS increases. Similar to other types of rocks where PPDs are more consistent as shown in **Figure 3.47**, compared with SST, with the increase in the confining stress. Moreover, MCS, YM, and PR increase as the confining stress increases.

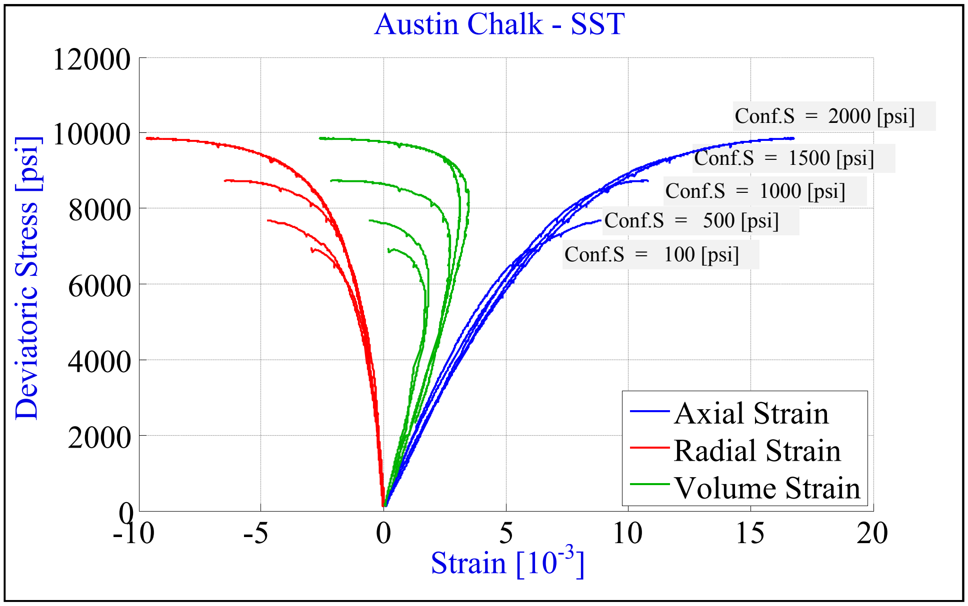

Figure 3.40: The fountain plot of all the single stage triaxial tests performed on the Austin Chalk against axial, radial, and volume strains.

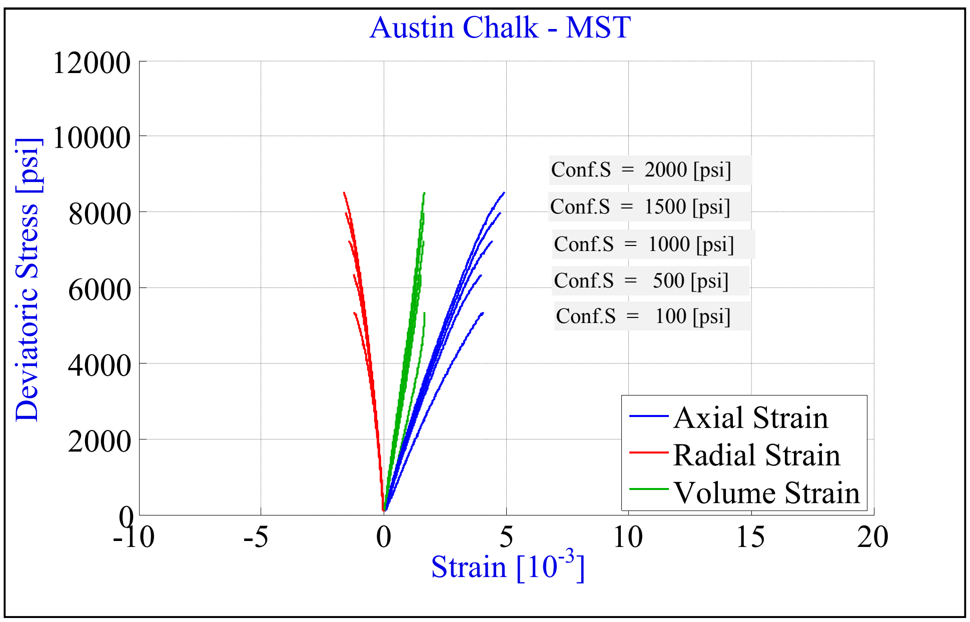

Figure 3.41: The fountain plot of the multistage triaxial test performed on the Austin Chalk against axial, radial, and volume strains.

3.4.2 Young's Modulus

Similar to other types of rocks, in the SST the stiffness (slope of the stress/strain plot) increases as the confining stress increases except **Figure 3.42** shows the stiffness curves for the SST. **Figure 3.43** show the equivalent plots for the MST where the stiffness increases and more consistent with the increase in the confining stress.

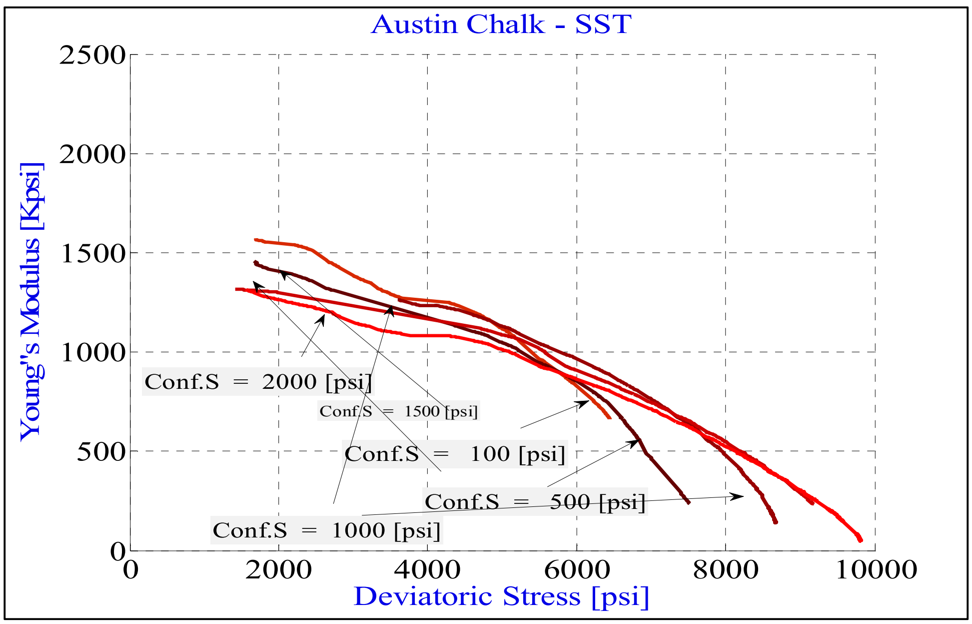

Figure 3.42: The stiffness for all single triaxial tests where it is clear that the stiffness decreases at 2000psi.

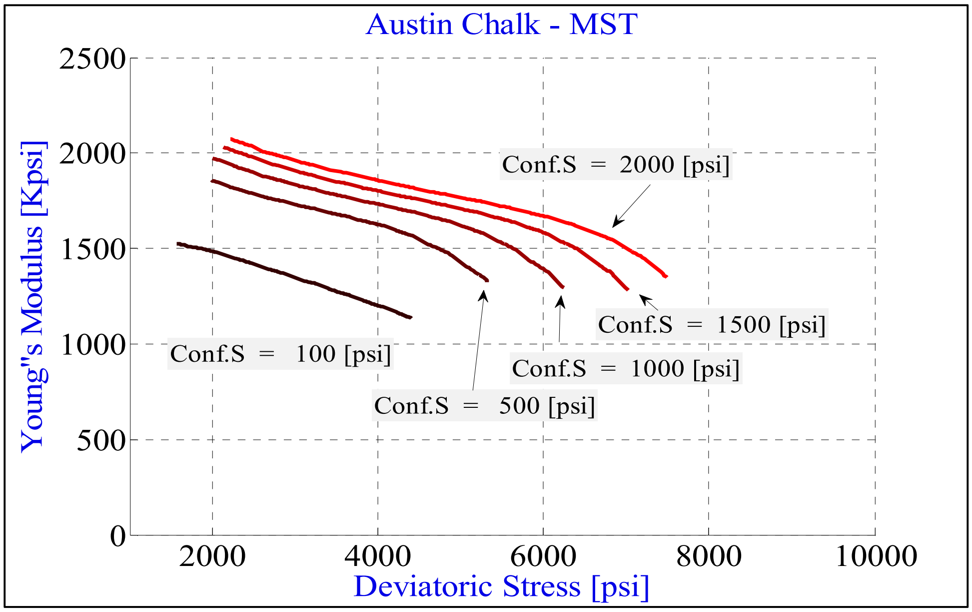

Figure 3.43: The stiffness of the multistage test where it increases as the confining stress increases.

3.4.3 Results Summary of Austin Chalk

The summary results are displayed in **Table 3-4** where a confining pressure from 100 to 2000 psi is applied in the SST and the same confining steps for MST. Therefore, we get more than three points to check the possibility to correct the properties obtained from MST to those obtained from SST.

Table 3-4: Results summary of Austin Chalk tests.

Conf. Stress [psi]	SST			MST		
	MCS [psi]	YM [Kpsi]	PR	PPD [psi]	YM [Kpsi]	PR
100	6948	1394	0.36	5353	1387	0.27
500	7682	1251	0.28	6343	1705	0.29
1000	8738	1276	0.24	7228	1765	0.3
1500	9354	1133	0.26	7982	1794	0.31
2000	9853	1076	0.22	8512	1830	0.31

As we notice from the table, this type of rocks is of intermediate strength, between the Miocene sandstone and the Shale. It also has a narrow range in properties and almost no stress dependence for the Young's modulus and Poisson's ratio measurements. **Figure 3.44** through **Figure 3.46** show the results of the mechanical properties of Austin Chalk.

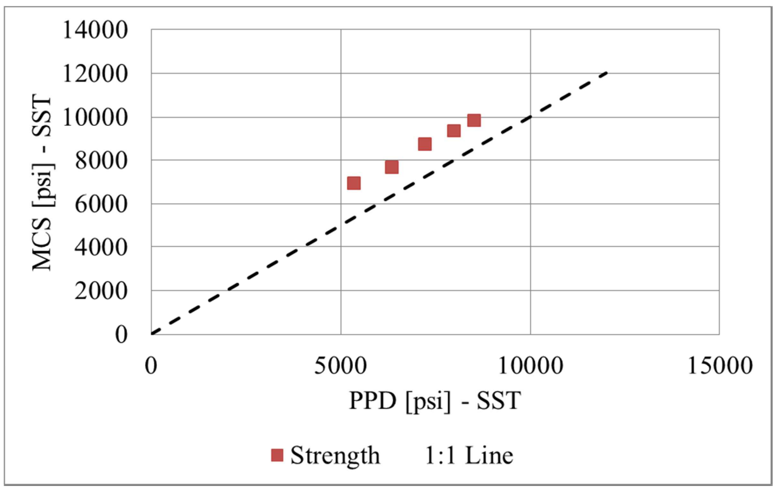

Figure 3.44: Strength comparison plot of for Austin Chalk. As with all the data the results are strongly correlated.

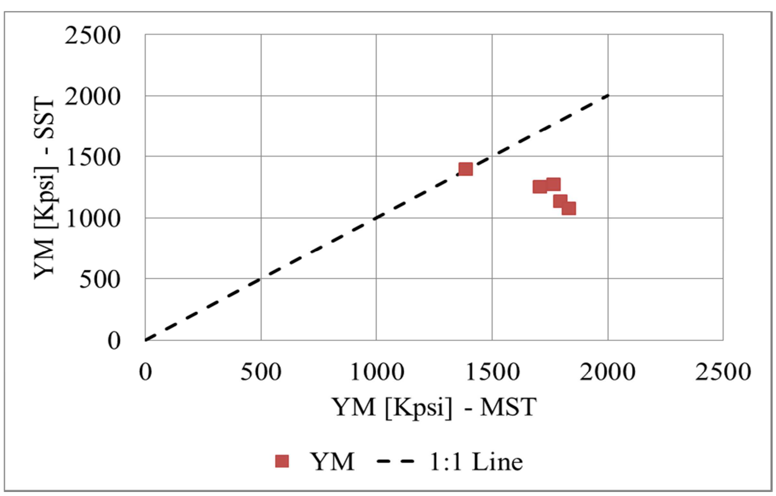

Figure 3.45: Comparison plot of Young's modulus for Austin Chalk. There is almost no dependence on confining stress. The variation for the one sample is thought to be due to sample heterogeneity

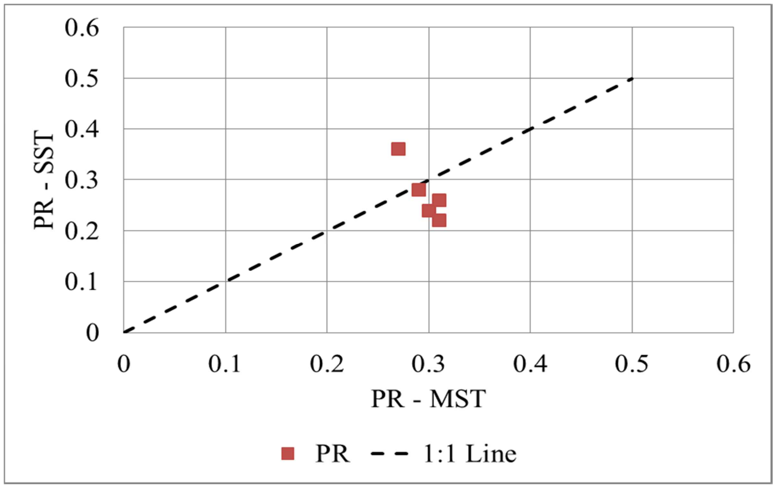

Figure 3.46: Comparison plot of Poisson's Ratio for Austin Chalk. The sample with low Poisson's ratio is the same sample with the largest Young's modulus in Figure 3.47.

The comparison between MST and SST for the p/q plot is shown in **Figure 3.47**. We notice that the MST is shifted down the SST. Similar to other types of rocks, the MST is always below of the SST as the PPD is lower than the MCS.

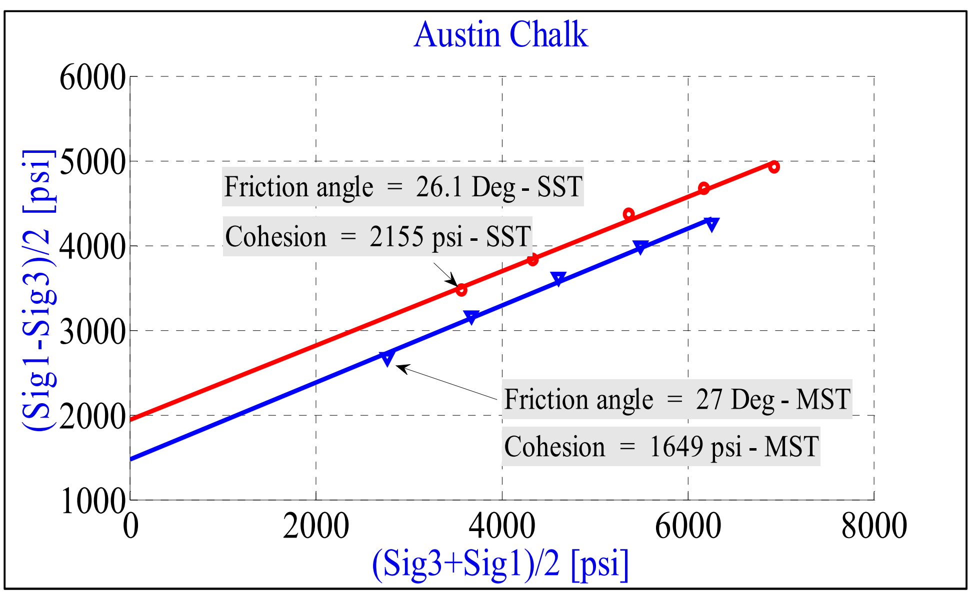

Figure 3.47: Comparison p/q plot of both single stage triaxial test and the multistage triaxial test.

3.5 Berea Sandstone

The Berea Sandstone was named for exposures near Berea, Cuyahoga County, where it was quarried at an early date for grindstones. The Berea is fine-grained, but the grains are angular rather than rounded, which makes this stone ideal as an abrasive. It is still quarried at South Amherst, where it reaches a thickness of more than 200 feet. Traditionally, the Berea was considered to be of Mississippian age but recently it has been assigned a Late Devonian age. The Berea formed when sand was carried by streams into the Ohio Sea from the Canadian Shield to the north and from the Catskill Delta to the east.

Figure 3.48 show a sample of the Berea Sandstone used in one of the tests. Due to the availability of this kind of rocks, five SSTs tests and one MST with five confining stress stages were applied to it where at each one, the rock didn't reach the cap stress and all data are still valid in the Mohr-Coulomb plot. The data shows a different type of behavior where the PPD what significantly lower than the MCS and the correction factor applied to it is bigger than the other types as we will see in the next chapter.

Figure 3.48: Berea Sandstone sample.

Figure **3.49** show an SST test applied to the sample at 1000 psi of confining stress. Two unload and reload cycles were applied to this sample where elasticity studies can be conducted in later work.

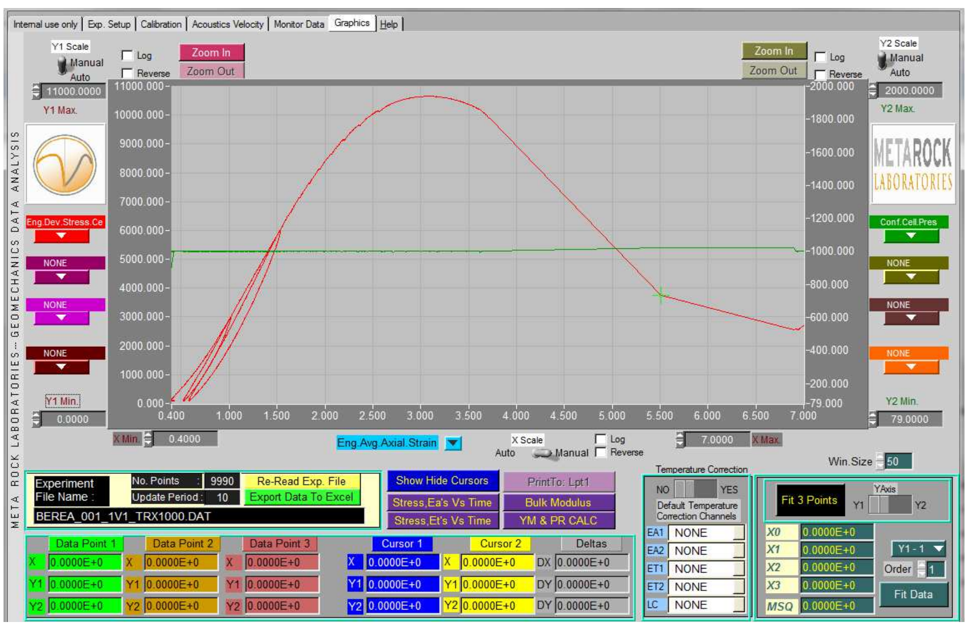

Figure 3.49: Single stage triaxial test is performed at 1000psi confining stress as displayed by the real time data acquisition system.

Moving to MST, **Figure 3.50** shows the behavior of the sample under different confining stress where, differ from the other rocks, the irrecoverable volume strain is approximately the same for all confining stages.

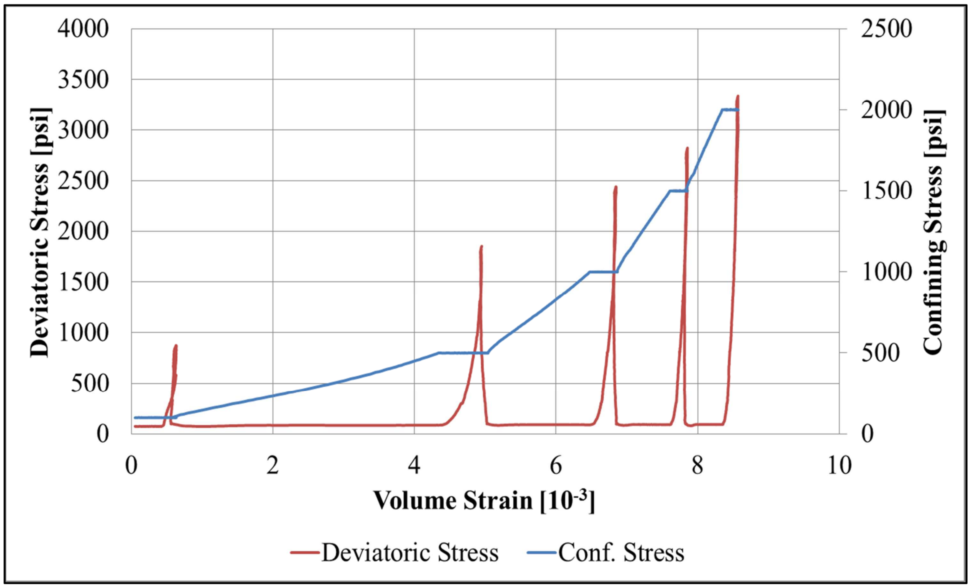

Figure 3.50: The deviatoric and confining stresses that are plot against volume strain.

3.5.1 Strength

This is the most interesting rock case in this study. Looking to the stiffness of these samples in **Figure 3.51** which is represented by the slope of the blue curves, we can notice that the last three samples (confining stress 1000-2000 psi) are significantly stiffer than the first two samples. Even with this difference in the stiffness a correction is still possible. It is thought that this large variability is due to the variation in the samples this will be confirmed through thin section analysis.

For the MST as shown in **Figure 3.52** we see the same behavior as shown in the other types of rocks except that the PPD is relatively smaller than the MCS comparing it to the other rocks we will result a higher correction factor as we will discover in the next chapter as well.

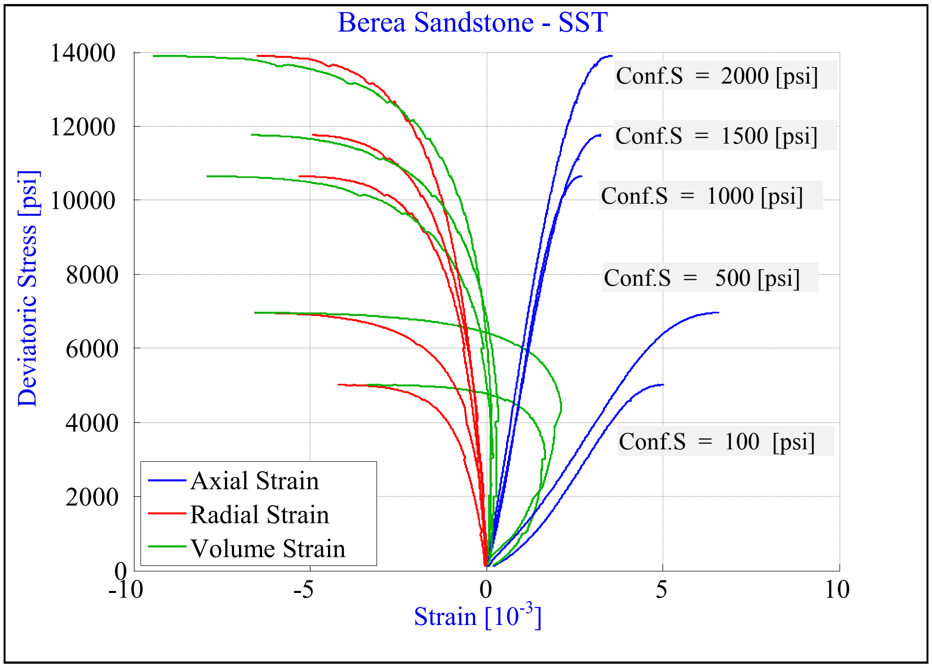

Figure 3.51: The fountain plot of all the single stage triaxial tests performed on the Berea Sandstone.

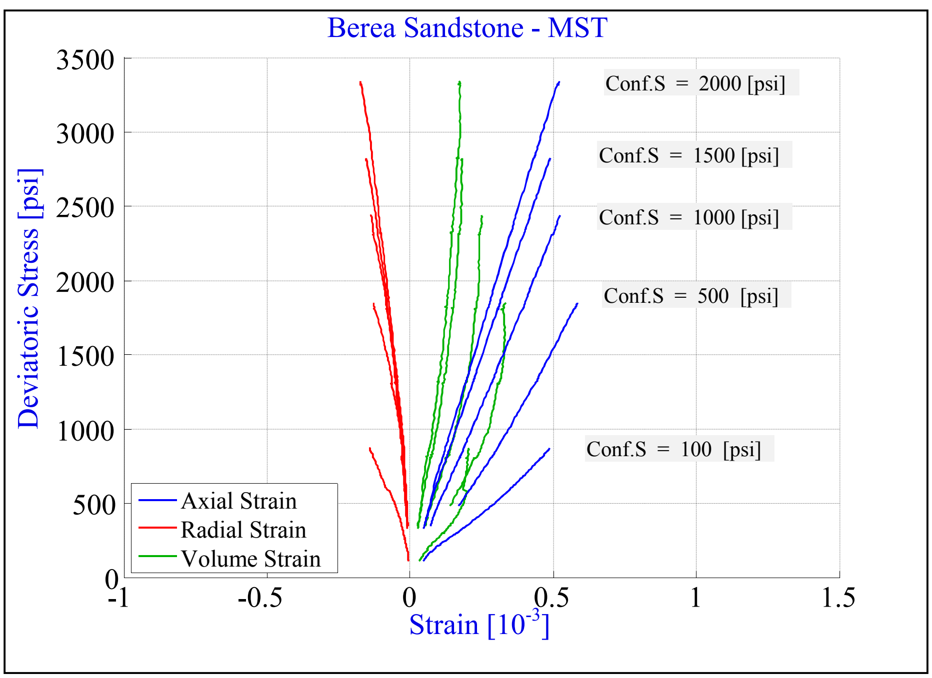

Figure 3.52: The fountain plot of the multistage triaxial test performed on the Berea Sandstone against axial, radial, and volume strains.

3.5.2 Young's Modulus

The difference in the stiffness is more noticeable when we plot the stiffness as it is shown in **Figure 3.53**. As we notice, form 100psi to 500psi of confining stresses the sample stiffness stands apart from the other data. Also the stiffness has a certain trend where it increases to a peak value that it starts decreasing until reaching the MCS.

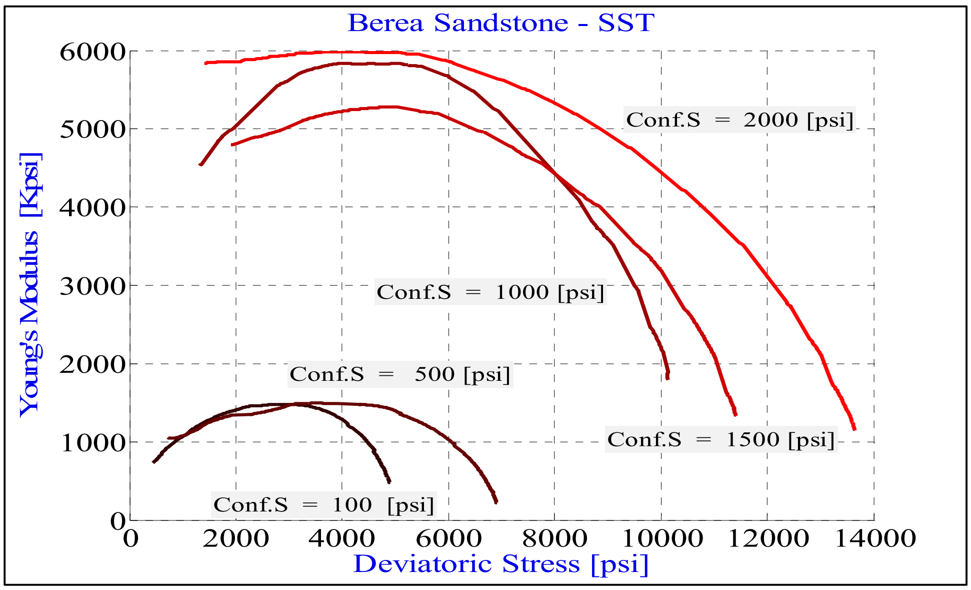

Figure 3.53: The stiffness for all single triaxial tests where it is clear that we have two types of the same rock that have different stiffness.

For the MST as PPDs have low values, the stiffness is approximately constant for all confining stresses and similar to other types of rocks the stiffness increases as the confining stress increases. **Figure 3.54** shows the stiffness trend for all the confining stresses.

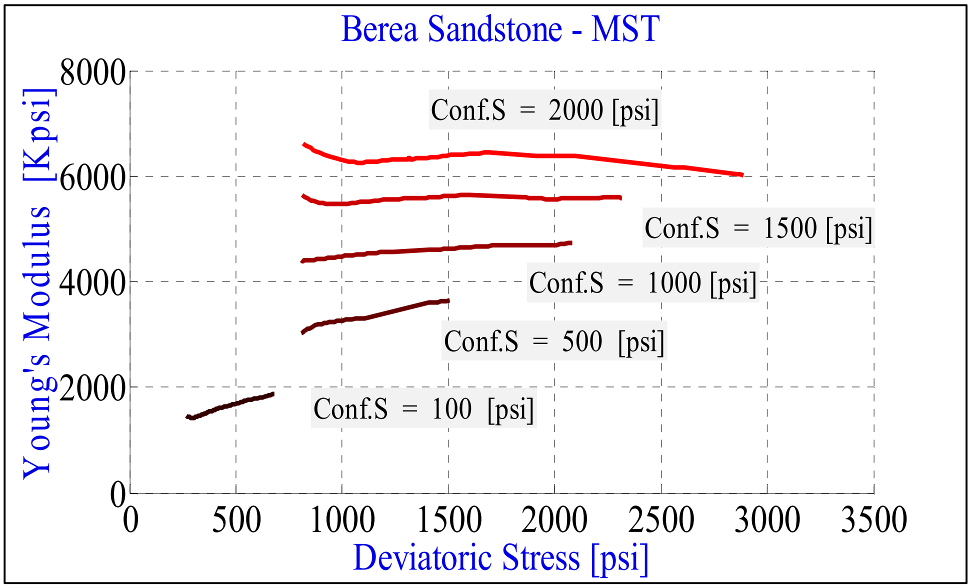

Figure 3.54: The stiffness of the multistage test where it increases as the confining stress increases.

3.5.3 Results Summary of Berea Sandstone

Saving the most interesting data for last, the Berea data stands apart. Young's modulus and Poisson's ratio both show significant increases with stress (Similar to the Miocene sandstone). **Table 3-5** shows the tests summary.

Table 3-5: Results summary of Berea Sandstone tests.

Conf. Stress [psi]	SST			MST		
	MCS [psi]	YM [Kpsi]	PR	PPD[psi]	YM[Kpsi]	PR
100	5015	1280	0.27	875	1546	0.25
500	6957	1347	0.15	1852	3171	0.17
1000	10650	4751	0.43	2440	4567	0.25
1500	11760	4724	0.23	2823	5593	0.31
2000	13898	5846	0.34	3340	6433	0.33

As the other types of the rocks and referring to Figures Figure **3.55** to Figure **3.57**, there is strong correlation between confining stress and strength.

Poisson's ratio and Young's modulus also show a correlation with confining stress similar to the results for the Miocene sandstone.

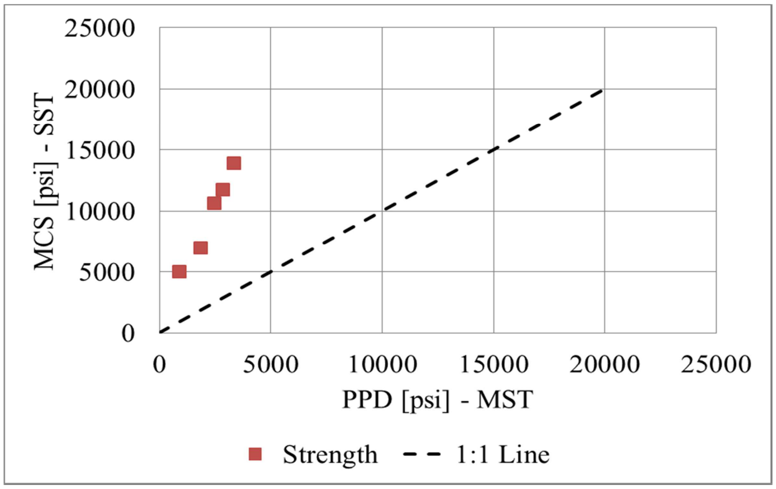

Figure 3.55: Comparison plot of the maximum compressive strength to the point of positive dilatency for Berea Sandstone where a linear correction factor can be found between PPD and MCS.

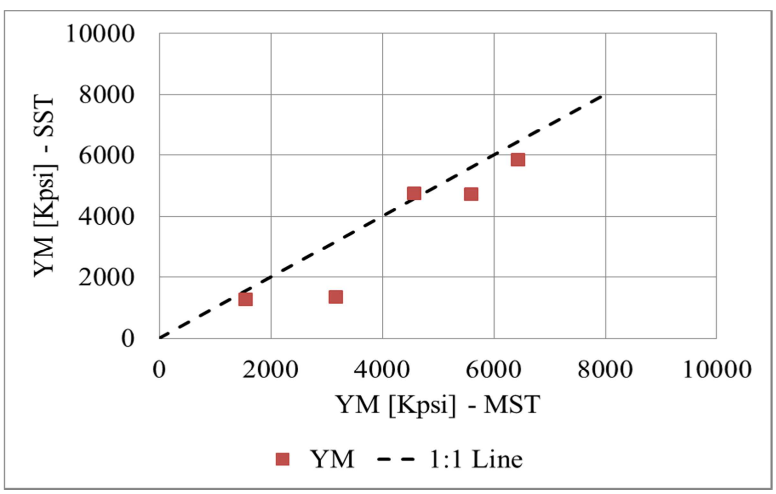

Figure 3.56: Comparison plot of Young's modulus for the Berea Sandstone, YM increases as the confining stress increases.

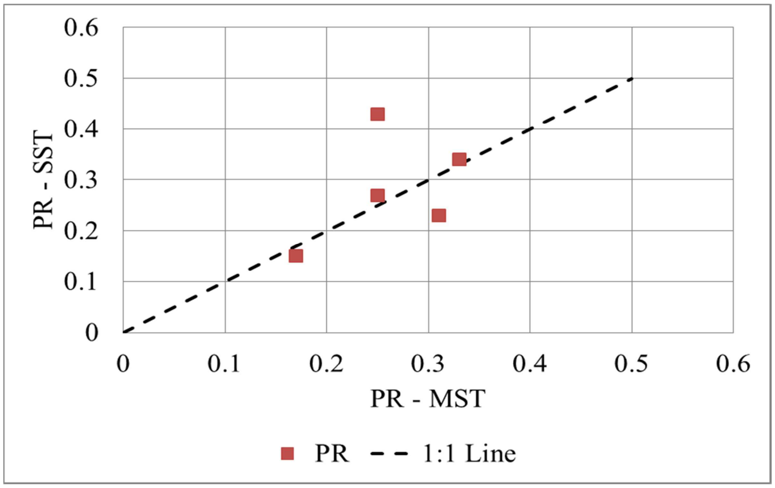

Figure 3.57: Plot for Poisson's ratio for comparing the results of the multi-stage test to the single stage tests for the Berea Sandstone.

Figure 3.58 shows the comparison between SST and MST on the p/q plot where different from the previous type of the rocks, the MST has significantly low values compared to the SST and the correction factor will be higher regarding the other rock types.

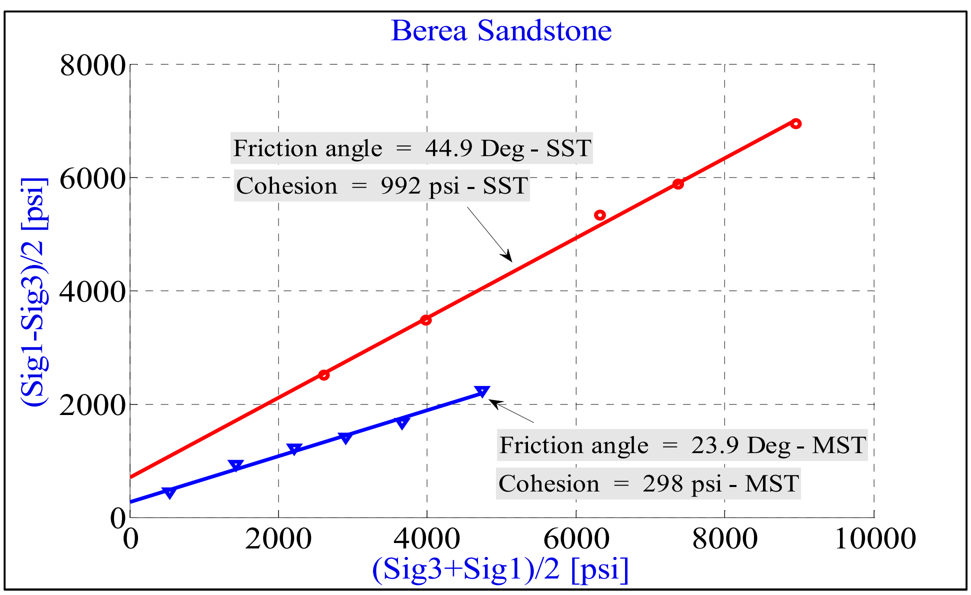

Figure 3.58: Comparison p/q plot of both single stage triaxial test and the multistage triaxial test.

Finally **Figure 3.59** shows the PPD to MST plot for the five types of the rocks. One correction factor can be used to correct PPD to MST where, for each rock type, there is a unique correction factor that we believe it is related to the mineralogy of the rock.

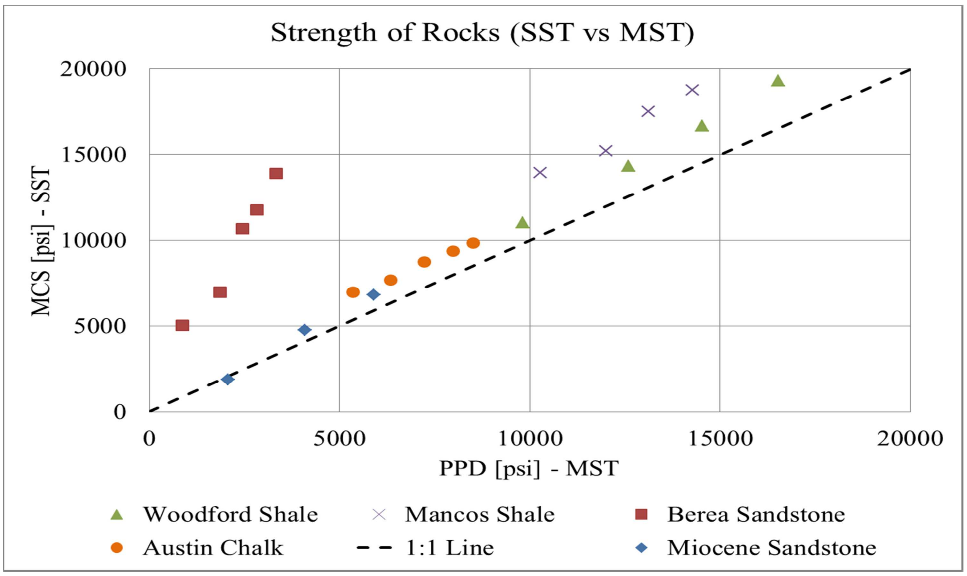

Figure 3.59: PPD to MST plot for the five types of the rocks where a correction factor can be found.

Chapter 4 : Summary and Conclusion

4.1 Correction Factor, Friction Angle, and Cohesion.

For the all the tests we performed on five different types of rocks, we found that there is a strong correlation between the positive point of dilatency determined from the MST and the maximum compressive strength determined from the SST This summary is shown in **Figure 3.59**. As expected the MCS always lies above the PPD for the MST. For all five data sets there exists a directly proportional relationship. Using one correction factor, we are able to correct PPD to MCS, and as a result, correcting the cohesion and friction angle from MST to SST.

The correlation takes the following form:

$$MCS = a * PPD, \qquad 4.1$$

where (a) is the correction factor given in [psi/psi]. The following table shows the correction factor and the correlation coefficient (R^2) for each type of rocks.

Table 4-1: Summary table of measured correction factor between the point of positive dilatancy derived from the multistage tests and the maximum compressive strengths from the single stage tests.

Rock Type	Correction Factor (a) [psi/psi]	R^2
Miocene Sandstone	1.137	0.976
Woodford Shale	1.149	0.995
Mancos Shale	1.315	0.960
Austin Chalk	1.196	0.919
Berea Sandstone	4.197	0.949

Figure **4.1** to Figure shows the plots of MCS vs. PPD where the continuous line shows the correction line in blue color. The dash line is the 1:1 line is used to compare the correction line against it.

We found that the correction best fits Sandstone and Shale. For Austin Chalk, the correlation has the lowest goodness of fit. We believe that this is due to the nature of the rock as it is belong to carbonates that has vuggy porosities that makes a heterogeneity of the samples in terms of strength within the same core.

Only for Berea Sandstone, the correction factor is large relative to other rocks where they have values close to each other that range from 15% to 30% of the PPD value. We can refer that to the nature of the rock type that leads to this high correction factor.

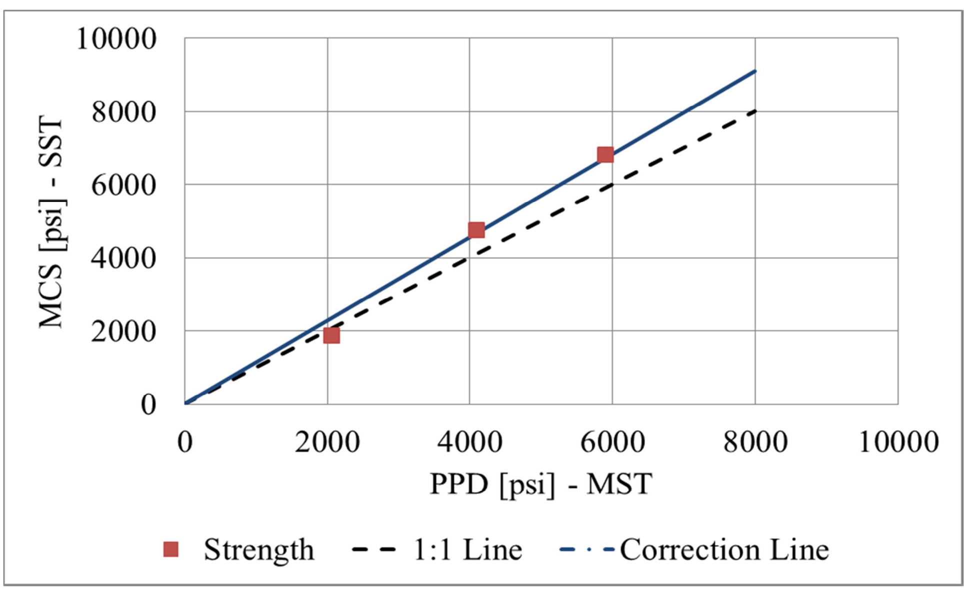

Figure 4.1: Miocene Sandstone correction line (blue) that has a factor of 1.137 with an R^2 of 0.976.

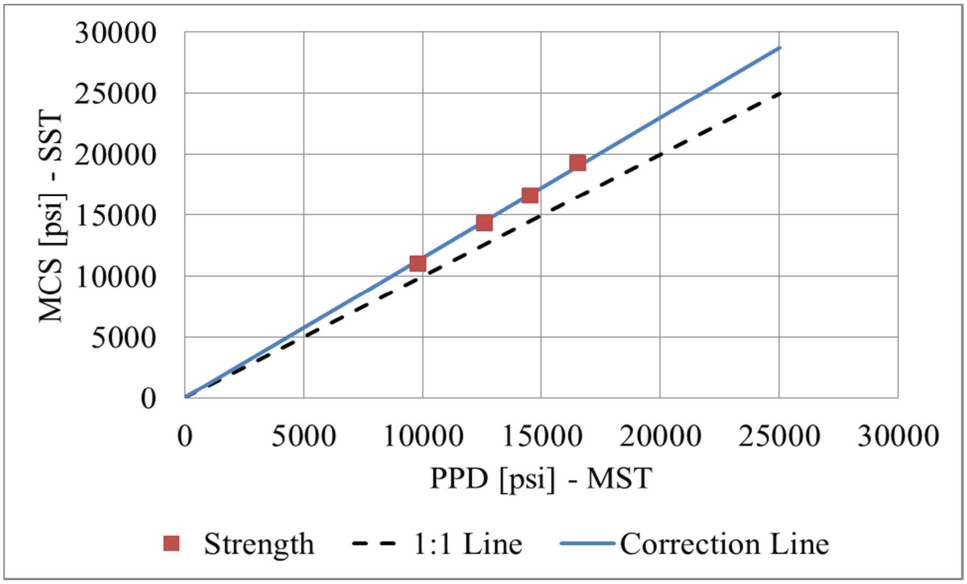

Figure 4.2: Woodford Shale correction line (blue) that has a factor of 1.149 with an R^2 of 0.995 (most fits).

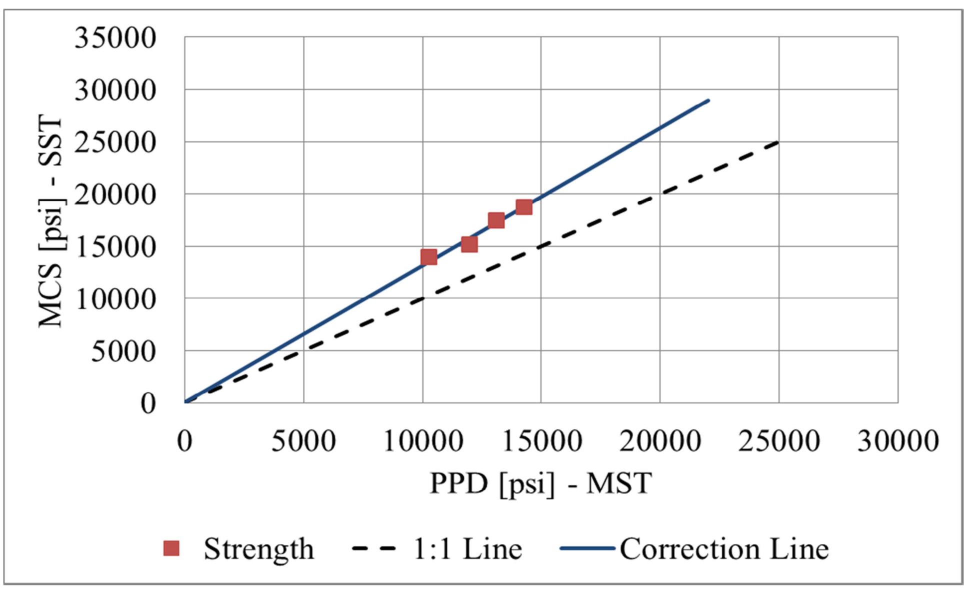

Figure 4.3: Mancos Shale correction line (blue) that has a factor of 1.315 with an R^2 of 0.96.

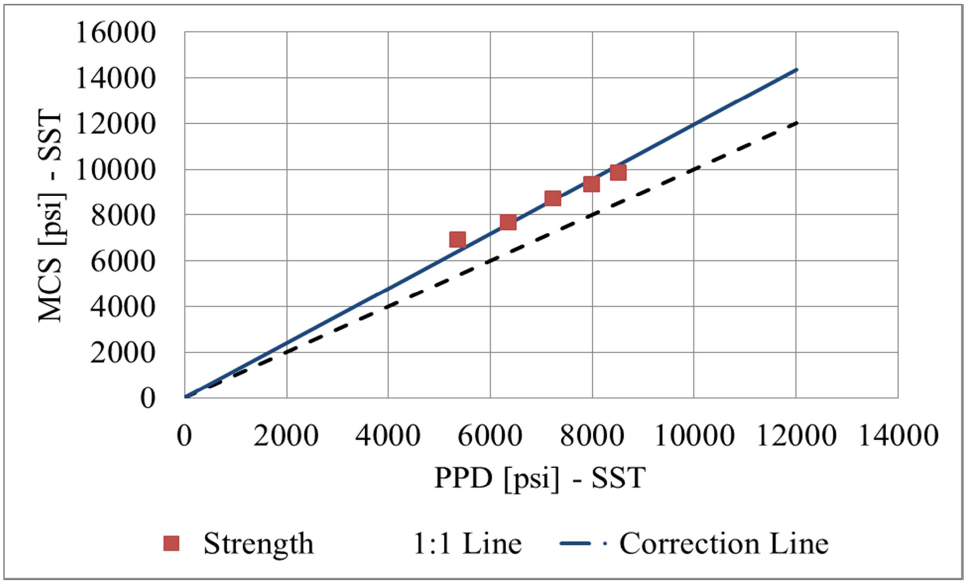

Figure 4.4: Austin Chalk correction line (blue) that has a factor of 1.315 with an R^2 of 0.919 (least fits).

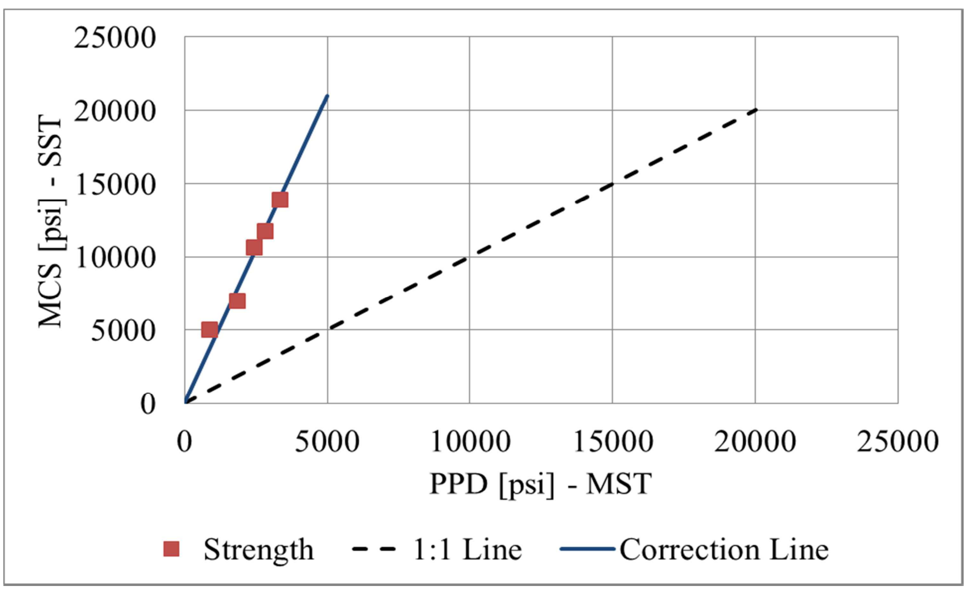

Figure 4.5: Berea Sandstone correction line (blue) that has a factor of 4.197 with an R^2 of 0.949, it has large correction factor relative to the others samples studied.

We are now comparing predicted maximum compressive strength versus the measured values including the friction angle and cohesive strength. The p/q plots for each type of rocks are shown in Figures Figure **4.6** to Figure **4.10**. The plot also shows the results of the predicted values from the multistage plots.

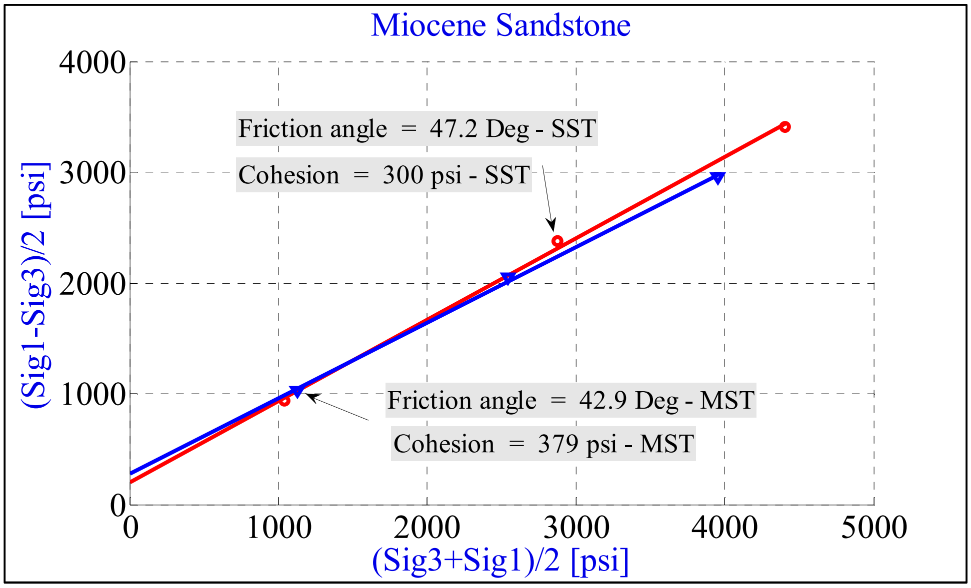

Figure 4.6: p/q plot for the single stage and the values predicted from multistage data for the Miocene Sandstone.

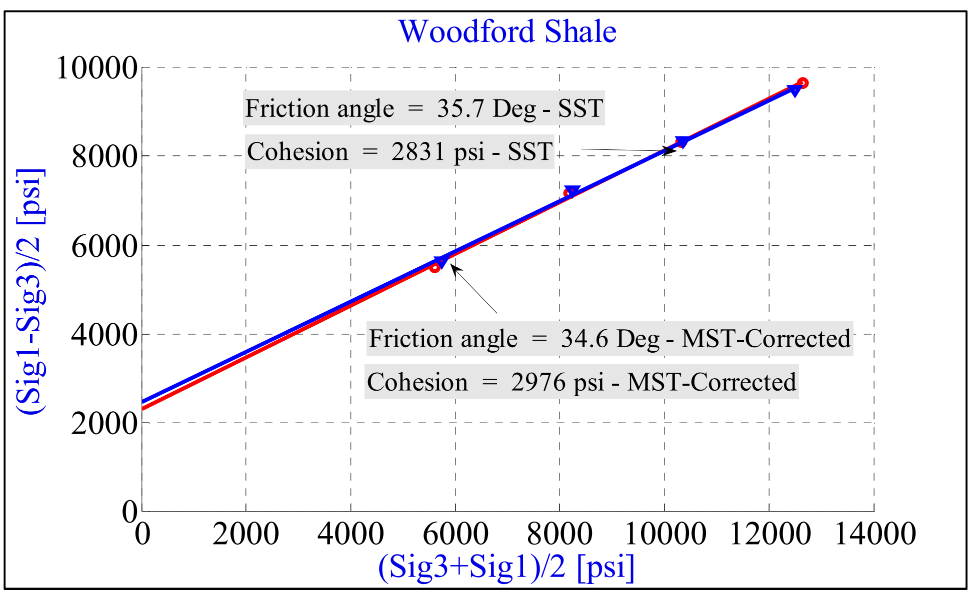

Figure 4.7: p/q plot for the single stage and predicted from multistage data for Woodford Shale.

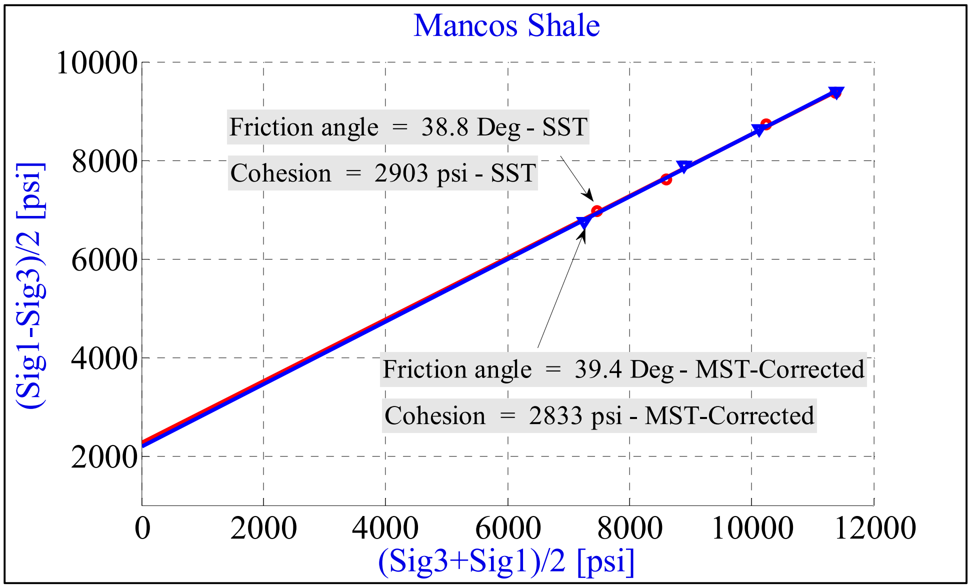

Figure 4.8: p/q plot for the single stage and predicted from multistage data for Mancos Shale.

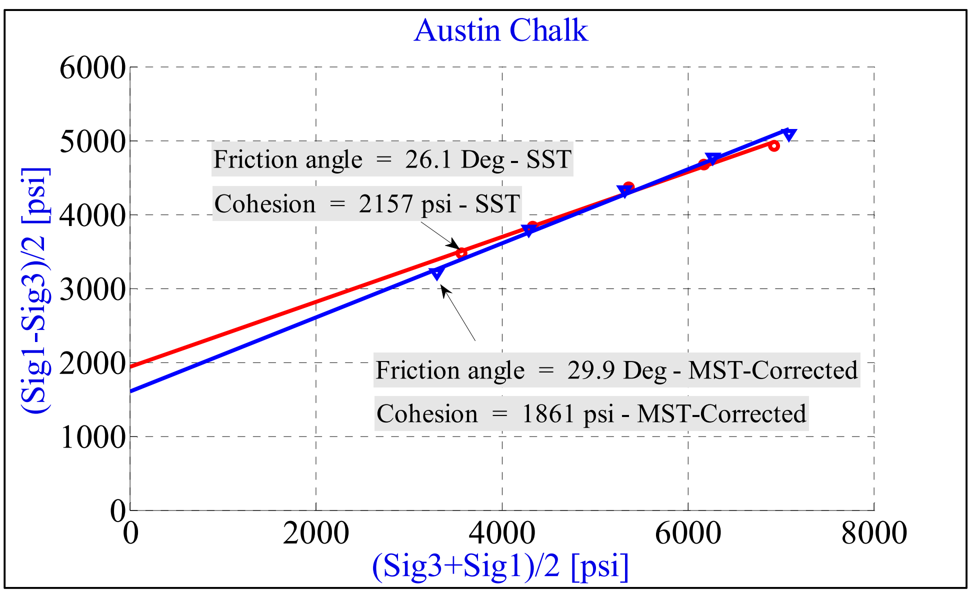

Figure 4.9: p/q plot for the single stage and predicted from multistage data for the Austin Chalk. The cohesion predicted is significantly different from the SST.

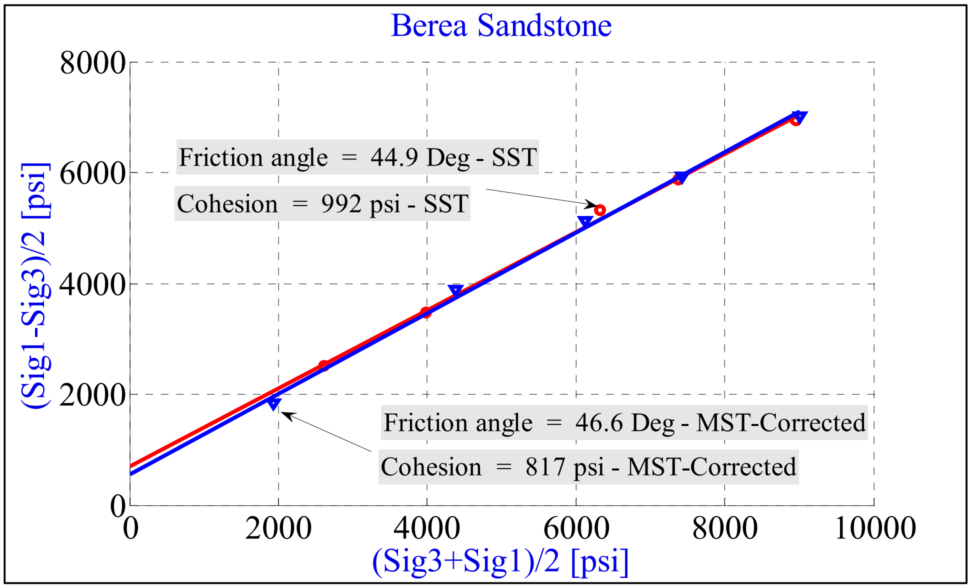

Figure 4.10: p/q plot for the single stage and predicted from multistage data for Berea Sandstone.

The results shown in the on the p/q plots of the rocks are summarized in **Table 4-2** where it shows the SST results, MST results, corrected MST, and the correction factor associated with each rock type.

Table 4-2 : Results for the predicted friction angle and cohesion from the multistage test and the measured friction angle and cohesion from the single stage tests.

Rock Type	SST		MST		MST_Corrected		Correction Coeff [psi/psi]
	Friction Angle [°]	Cohesion [psi]	Friction Angle [°]	Cohesion [psi]	Friction Angle [°]	Cohesion [psi]	
Miocene Sandstone	47.2	300	42.9	442	45.1	408	1.137
Woodford Shale	35.7	2831	32.3	2722	34.6	2976	1.149
Mancos Shale	38.8	2903	34.7	2389	39.4	2833	1.315
Austin Chalk	26.1	2157	27.0	1649	29.9	1861	1.196
Berea Sandstone	44.9	992	22.5	334	46.6	817	4.197

Now, the plots of the measured values (SST) are plotted against the predicted values (corrected MST) as shown in figures **Figure 4.11** (for friction angle) and **Figure 4.12** (for cohesion).

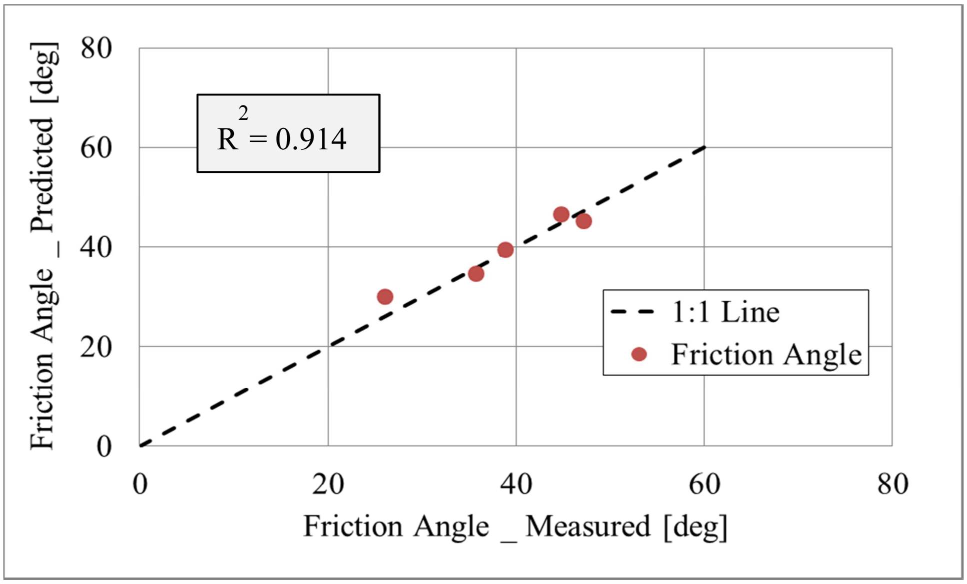

Figure 4.11: Predicted versus the measured friction angle using the individually correction factor for each type of the rocks.

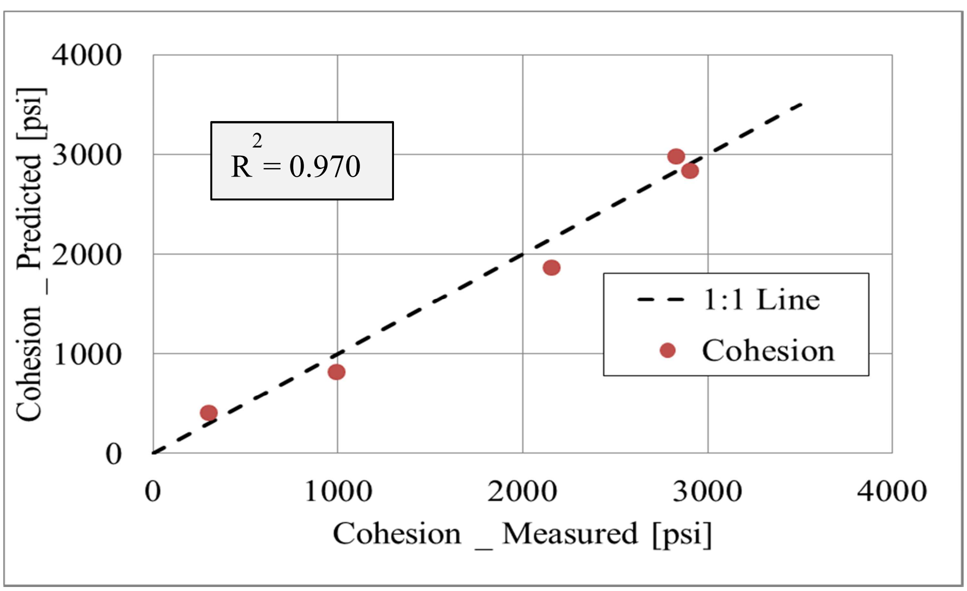

Figure 4.12: Predicted versus measured cohesion using the individually correction factor for each type of the rocks.

The results are shown in **Table 4-3** for using the average correction factor of 1.2. We have omitted Berea because it obviously does not fit with the rest of the data.

Table 4-3: Values for the cohesion and friction angle using an average value of the correction factor.

Rock Type	SST		MST		MST_Corrected			
	Friction Angle [^{o}]	Cohesion [psi]	Friction Angle [^{o}]	Cohesion [psi]	Friction Angle [^{o}]	Cohesion [psi]	Correction Factor [psi/psi]	Averaged Factor [psi/psi]
Miocene Sandstor	47.2	300	42.9	442	43.9	492	1.137	1.20
Woodford Shale	35.7	2831	32.3	2722	35.4	3058	1.149	
Mancos Shale	38.8	2903	34.7	2389	37.8	2677	1.315	
Austin Chalk	26.1	2157	27.0	1649	30.0	1864	1.196	

The results of using the average values of 1.2 for the correction factor are plotted in **Figure 4.13** and **Figure 4.14**. We see that the results slightly deviate more in case of the friction angle and little more that is noticeable in case of the cohesion. However the results are still well within the variability that we would expect from a repeated use of the SST protocol.

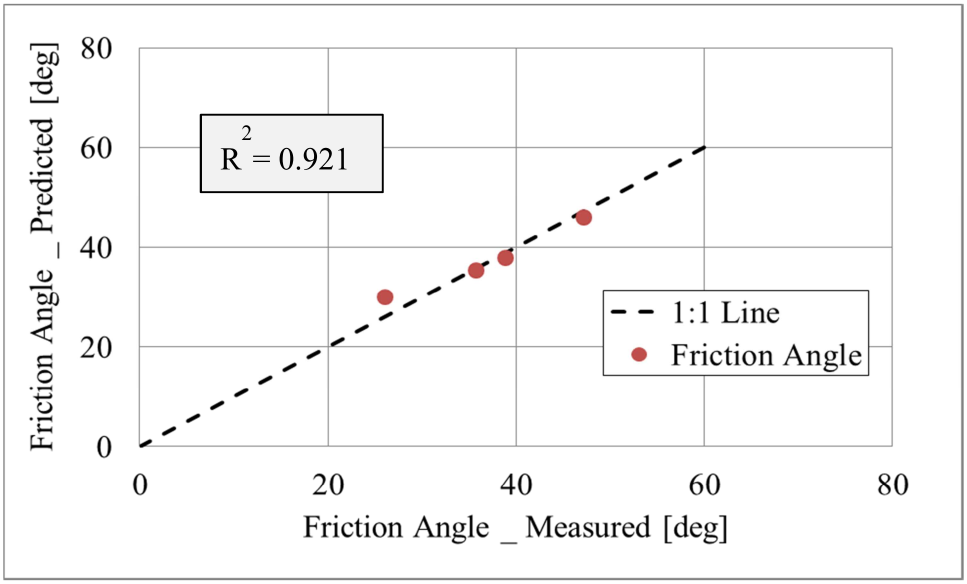

Figure 4.13: Predicted versus the measured friction angle using the average correction excluding Berea Sandstone.

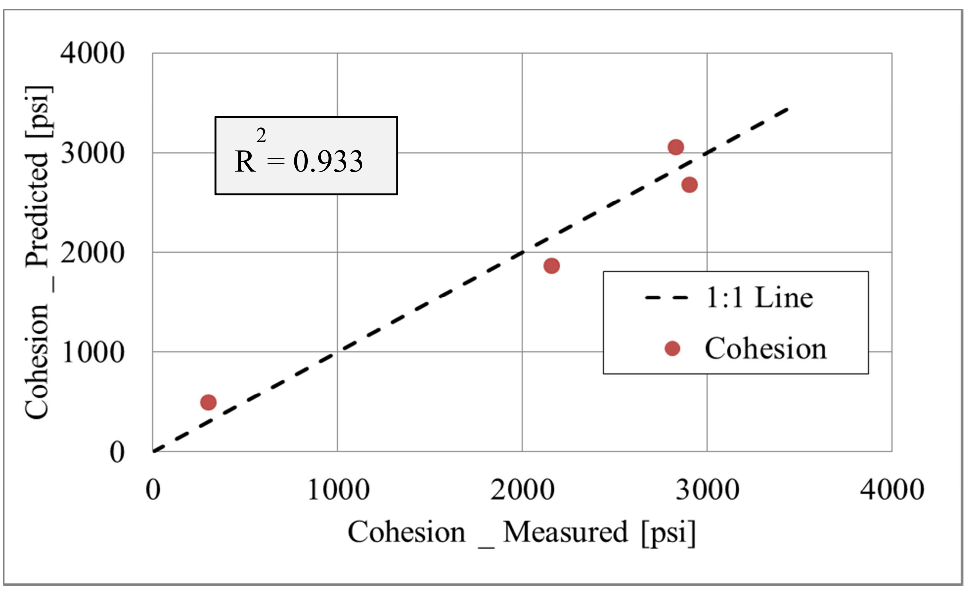

Figure 4.14 Predicted versus measured cohesion using the average correction excluding Berea Sandstone.

4.2 Conclusions

We have established a simple directly proportional relationship between MCS for single stage tests and the PPD for multistage tests. The sample set included two Sandstones, two Shales, and a Carbonate (Chalk). This allows an estimate of friction angle and cohesion to be performed using a single test multistage test. This technique conserves core material and significantly reduces the problem of obtaining suitable twins.

The range in Young's modulus was from 200,000 to several million. The maximum compressive strength ranged from 2000 to 20,000 psi. Using individual correction factors the correlation coefficients were all above r^2 of .92. Using a single average correction factor (1.2) the correlation coefficients were all above all above r^2 of 0.9.

As expected we see increased scatter in the predicted cohesion and friction angle when we use an average correction factor. However the scatter in the predicted values is comparable to the scatter we would we find by repeating the single stage measurements on a twinned sample set.

This study shows only a weak relationship between the PPD related to SST and the PPD of the MST. This is similar to the variation in other rock properties measured using the single stage tests. In contrast, an even more interesting question is why there is such a strong correlation with the maximum compressive strength from the single stage tests. It is inferred that this is a stable rock property than these other measured parameters.

The PPD was chosen as the reference point for the SST because it is a unique, unambiguous point that is relatively insensitive to operator interpretation. It also represents a stress level where relatively little damage having been done to the sample. This is evidenced by the high level of correlation achieved in the study. This low level of damages is thought to also be due to the stress path followed. The deviatoric stress is removed before the confining stress is raised at almost zero deviatoric stress. There the micro-cracks are closed and the next axial stress ramp started with the most stabile initial conditions possible.

Further work is needed to understand the response of the Berea Data. The samples measured appeared to divide in two sets of data however using either of the data sets still gave a significantly different correction factor from the rest of the sample. These failures were much more ductile than the rest of the data (i.e. a large difference between the PPD and MCS). We attribute this to mineralogical differences between these samples. This is currently under investigation.

.

References

1. N-Y. Chang, E. J. B. (1979). "Oil Shale Strength Characterization Trough Multiple Stage Triaxial Tests."

2. Nien-Yin Chang, A. L. J. (1978). "Multiple-Stage Triaxial Test on Oil Shale."

3. A. Taheri, K. T. (2008). "Proposal of a New Multiple-Step Loading Triaxial Compression Testing Method."

4. Koichi Akai, Y. O. D.-H. L. (1981). "Improved Multiple-Stage Triaxial Test Method for Soft Rock."

5. Adrian M.Crawfor, D. A. W. (1987). "A Modified Multiple Failure State Triaxial Testing Method."

6. John Conrad Jaeger, N. G. W. C., Robert Zimmerman (2007). "Fundamentals of Rock Mechanics, 4th Edition."

7. E. Fjaer, R. M. H., P. Horsrud, A.M. Raaen & R. Risnes (2008). "Petroleum Related Rock Mechanics." Elsevier.

8. Blümel, M. (2010). "Comparison of Single and Multiple Failure Triaxial Tests." ISBN 978-0-415-80481-3.

9. Ron Martin, J. B., Raj Malpani, Garrett Lindsay, and Keith Atwood (2011). "Understanding Production from Eagle Ford-Austin Chalk System." SPE.